Observational Tracers of Galaxy-Merger Remnants

A Senior Thesis

Submitted to Princeton University in partial fulfillment of the requirements
of the A.B. degree in astrophysics.

by

Jeremy S. Heyl

I hereby declare that I am the sole author of this thesis. I authorize Princeton University to lend this thesis to other institutions or individuals for the purpose of scholarly research.

Jeremy S. Heyl '92

I further authorize Princeton University to reproduce this thesis by photocopying or by other means, in total or in part, at the request of other institutions or individuals for the purpose of scholarly research.

Jeremy S. Heyl '92

Princeton University requires the signatures of all persons using or photocopying this thesis. Please sign below, and give your address and the date.

Acknowledgements

I would like to express my thanks to my sister, Rebecca, my mother, Carole, and my father, George for their support throughout the years. I must recognize the late Yoram Avni under whom I took my first astrophysics class. At Princeton, I thank my friends who nodded knowingly as if they understood what I was talking about; I thank Robert Lupton, Jill Knapp and Jim Gunn for their years of encouragement and confidence; I thank David Spergel and Lars Hernquist without whom this work would have not been possible. I thank Martin Schwarzschild and Sandra Faber for their insights and elucidating conversations. I thank the Dean of the College for a grant from the Senior Thesis Roundtable Fund to support research at the University of California at Santa Cruz.

And finally I express my gratitude to Nature who has put a surprise under every rock and inside every galaxy as the case may be. Thank you all.

Abstract

This senior thesis examines the expected observational properties of galaxy-merger remnants by analyzing the results of large numerical simulations of galaxy collisions. It is found that the deviations of isophotes from ellipses (boxiness or diskiness) depends strongly on the initial conditions and in some of the remnants no deviations are found in the $a_{\cos 4\theta}$ term at all within the errors of the analysis. By modeling the color gradients in progenitors, we calculate the gradients in the remnant. During the merger, they are weakened substantially, but still only fall short of the gradients observed in elliptical galaxies by a factor of a few. Furthermore, the remnants are examined for kinematic tracers, such as counterrotating cores and disks (both of which are present). However, more subtle features are present as well, such as a startling increase of v_r / σ with radius along the major axis of the remnant as viewed from certain angles. Additionally, we discuss the question of how the high central phase-space densities in elliptical galaxies can be achieved through mergers. By calculating how short the central phase-space densities of the remnants fall, we determine how much gas is needed in the progenitor galaxies to fuel enough star formation to produce the observed central densities of ellipticals.

Although the simulated merger remnants resemble elliptical galaxies in many qualitative features, quantitatively they do not, especially due to a shortfall in the central phase-space densities of the remnants. Therefore, we

conclude that the ordinary spirals of today cannot merge to form the ordinary ellipticals of today, opening the question of where are all the merger remnants hiding, or maybe that the merger rate over the history of the universe has consistently been overestimated.

Table of Contents

Acknowledgements i

Abstract ii

Table of Contents iv

Chapter 1: Introduction and Summary 1
- Overview 1
- General Properties of Elliptical Galaxies 1
- Formation Scenarios 3
  - Dissipative collapse 3
  - Dissipationless collapse 4
  - The merger hypothesis 5
- The Value of Simulations 8
- The Current Simulations 9
  - The method 9
  - Initial conditions 11
- Bibliography 16

Chapter 2: Isophotes 19
- The Predictions 19
  - Finding the isophotes 21
  - Distribution of ellipticities 25
  - Distribution of "boxiness" 29
- The Observations 32
- Reconciliation 33
- Bibliography 35

Chapter 3: Color Gradients in Merger Remnants 36
- Some Predictions 37
  - Phase mixing 37
  - After the merger 38
- Initial Color Gradients 40
  - The Andromeda model 40
- The Results of the Simulations 41
- The Observations 44
- Conclusion 47
- Bibliography 48

Chapter 4: Velocity Mappings of Merger Remnants 49
- The Transfer of Angular Momentum 50

Hierarchial transfer 51
Dark halos and angular momentum 51
The point-mass approximation 52
Misalignment of Kinematic Axes 56
Counterrotating cores 58
Velocity Dispersion and Rotation 59
A Preliminary Model of NGC 4550 61
Conclusion 63
Bibliography 64

Chapter 5: The Phase-Space Density Problem 65
Why is There a Problem? 66
Phase Densities in the Simulated Remnants 67
Gas Dynamics 68
A Very Much Simplified Gas Dynamical Model 68
How much gas? 71
Conclusion 71
Bibliography 74

Chapter 6: Concluding Remarks 75
Getting Mergers to Work 75
The Importance of Mergers in Galaxy Evolution 76
Further Research 77
Analysis 77
Simulations 78
Observations 79
Conclusion 80
Bibliography 81

Appendix A: Russian Sources in the Area 82
Initial Works 82
Collisionless Collapse 84
Observations 86

How Important Are Interactions? 87
Summary 88
Bibliography 89

Chapter 1: Introduction and Summary

Overview

Recent years have seen the development of CCD imaging and supercomputers, which has opened up entirely new areas of study in astrophysics, including "computational" astrophysics. This work, using these newly available tools, predicts the observational tracers of merger remnants and examines the hypothesis that elliptical galaxies form during the merger of spiral galaxies. We performed a series of numerical simulations of colliding spiral-like galaxies both with and without bulges and tried to take a few steps into the vast multi-dimensional space of the collision parameters. The results of these simulations were then compared with recent observations of the isophotes, color gradients, velocity distributions, and phase-space densities of elliptical galaxies, observations which would have been extremely difficult if not impossible more than a few years ago.

General Properties of Elliptical Galaxies

In recent years our view of elliptical galaxies has change markedly. Before the advent of CCDs the small-scale structure of ellipticals was nearly inaccessible. Ellipticals in the main were seen as nearly featureless distributions of stars with nearly perfect elliptical symmetry; the only descriptive parameter of their shape was ellipticity. Their flattening was thought to be caused by simple rotation. Furthermore, ellipticals were found

to have a nearly universal distribution of surface brightness - the de Vaucouleurs or $r^{1/4}$ law (de Vaucouleurs 1948); so universal that the $r^{1/4}$ law has nearly become a canonical definition of elliptical galaxies (de Vaucouleurs 1988).

However, there were hints that things were not so simple. Evans (1951) observed the twisting of the isophotes of NGC 1549, pointing to the now accepted notion that large elliptical galaxies are in general triaxial distributions of stars supported by an anisotropic distribution of velocities rather than by rotation as was previously believed. In the seventies, this picture of elliptical galaxies as rotationally flattened oblate rotators was torn asunder (Binney 1976; Binney 1978). Observations showed that the rotational velocities of large elliptical galaxies were one-third what would be expected from their flattening (Bertola and Capaccioli 1975; Illingworth 1977).

As the observational techniques and technology improved in the eighties, even more fine structure was discovered in ellipticals. Bender *et. al.* (1987), and Simien and Michard (1990) measured "boxy" and "disky" isophotes in ellipticals. Soon astronomers speculated that these rather common anomalies were traces of the formation of elliptical galaxies (Bender *et. al.* 1989). More recently, groups have measured the color gradients (Franx and Illingworth 1990; Peletier *et. al.* 1990) and the velocity distributions (Rix and White 1992; Franx *et. al.* 1989) in elliptical galaxies. The numerical simulations of galaxy mergers make predictions that can be compared with these recent

observations. Thus, we can start to evaluate the importance of mergers in the morphology of galaxies observed today.

Formation Scenarios

The avenues for the formation of elliptical galaxies may naturally be divided into dissipative and dissipationless scenarios, *i.e.* models in which hydrodynamics does and does not play a role. A more detailed and thorough review than that presented here may be found in Larson (1990).

Dissipative collapse

Larson (1970) proposed that spherical galaxies form during the collapse of clumpy and turbulent protogalaxies. These large clouds consisted of smaller clouds with large random motions up to the scale of the protogalaxy as a whole. As the protogalaxy collapsed, the random motions of the gas quickly dissipated on a timescale comparable to the dynamical time scale of the system, and star formation quickly ensued. Using the Salpeter initial mass spectrum and the assumption of instantaneous metal recycling, Larson's models resulted in galaxies closely resembling spheroids; furthermore, they predicted strong radial gradients in metallicity and the nearly complete conversion of gas into stars.

In the later models of Carlberg (1984), the constraint of spherical symmetry was removed. The simulations began with an initially flattened (2:1) spheroid with a uniform density of gas. The spheroid collapsed into a sheet with about half of the gas mass forming stars, and then this sheet

collapsed radially, and the remaining gas formed stars. This final violent relaxation resulted in an anisotropic, slowly rotating elliptical galaxy. These models also predicted radial gradients in metallicity, albeit much less steep than those found in Larson's models.

Dissipationless collapse

In contrast to the dissipative models described above, in a dissipationless collapse, star formation is presumed for the most part to have occurred before the protogalaxy begins to collapse. This model was first elucidated in a classic paper by Lynden-Bell (1967). He found that a distribution of stellar orbits could relax to statistical equilibrium if the stars passed through regions in which the gravitational potential was changing violently. This violent relaxation occurs without encounters between the stars and therefore is collisionless, and the rapidly changing potential of a collapsing protogalaxy provides an excellent venue for this process.

Villumsen (1984) and van Albada (1982) have explored the process of dissipationless collapse more recently. They found that systems with chaotic or asymmetric initial conditions will experience the effects of violent relaxation more strongly than spherically symmetric systems. Van Albada used a spherically symmetric distribution of smaller spherical clumps, while Villumsen started with uniform disk and bar-shaped arrangements. Through simulation, they both found that these initial conditions evolved, under the influence of gravity only, into objects resembling elliptical galaxies.

The merger hypothesis

The merger hypothesis in a way bridges these two avenues. As far as the stars are concerned the merger of two spiral galaxies is practically collisionless, but as spirals often contain appreciable amounts of gas one expects dissipative processes to also play a role. Furthermore, a merger creates a rapidly changing potential, conducive to violent relaxation. The merger hypothesis developed out of work studying the formation of bridges and tails during encounters of galaxies through the action of gravity alone, a idea that was revived by Pfleiderer and Seidentopf (1961) and Pfleiderer (1963).

Tashpulatov (1969, 1970) simulated the motion of test masses in the combined gravitational potential of a passing point mass and a rotating elliptical galaxy. The point masses were released from the vertex of the elliptical at progressively later times during the encounter. He found that the test masses formed narrow features resembling the bridges and tails observed in interacting galaxies. Later, Toomre and Toomre (1972) performed a more extensive set of simulations, calculating the motion of many test masses arranged in concentric, coplanar rings surrounding a point mass during a encounter with a second point mass. They also noted the formation of bridges and tails and compared the layout of the intermediate steps in the simulations with galaxies in the Arp Atlas (1966). Important for the merger hypothesis was their estimate of the number of "very old tumbled remains that one should see today." Assuming that merging pairs of galaxies only retain their tails and

other obvious observational symptoms of encounters for about 10^9 years, one would expect at least 10 times as many remnants from collisions over the past 10^{10} years. Moreover, one would expect mergers to have been more frequent in the early universe increasing this ratio further.

Toomre (1977) later more carefully calculated the expected number of merger remnants among the NGC galaxies. Using the assumption that merging pairs travel along loosely bound ellipses and that the initial distribution of binding energies was flat, he estimated that the merger rate has been proportional to $t^{-5/3}$ during the history of the universe. Furthermore, he tried to judge the bias produced by the fact that merging galaxies may be substantially brighter than their progenitors. His final estimate was that 250 of the NGC galaxies were likely merger remnants, whereas about 320 of the NGC galaxies have been classified as cE or E and about 290 as S0 in the *Second Reference Catalog* (de Vaucouleurs, de Vaucouleurs, and Corwin 1976). Toomre concludes, "All in all, if several hundred merged remnants of former disks do not now constitute many of the ellipticals, where else have they possibly gone?" Vorontsov-Vel'yaminov (1977) performed a calculation similar to Toomre's and estimated that the number of encounters between galaxies since the beginning of the universe was approximately equal to the total number of galaxies. He concludes, "This is a quantity which one cannot neglect neither in cosmogony nor in cosmology."

However, the merger hypothesis has some strong arguments against it.

First is the discrepancy between the central phase-space density in spiral disks and elliptical galaxies (Carlberg 1986). Not considering the bulges, the central phase-space density of spirals falls short of that of ellipticals of similar luminosities on average by factor of about 100. During a purely stellar dynamical interaction, the peak macroscopic phase-space density can only decrease or remain the same. The merger of spiral galaxies with gas may alleviate this problem. Second is the ratio of the number globular clusters to luminosity in ellipticals and spirals. Ellipticals are observed to have many more globulars per unit luminosity than spirals (van den Bergh 1990); and unless mergers can spark waves of globular-cluster formation, the hypothesis does not measure up. Again the addition of gas may solve this difficulty as well, but with each addition of gas the merger hypothesis resembles more and more the dissipative collision of gas clouds. A third reservation is philosophical, first presented by Ostriker in 1980. If all ellipticals are formed through mergers then how did the bulges of spirals, which are considered to be the low-mass extension of the family of elliptical galaxies, form? Finally, Toth and Ostriker (1992) argue that spiral disks cannot survive if they have absorbed more than a few percent of their mass through mergers within the lifetime of typical disk stars. This conclusion questions the estimates of Toomre (1977) and Vorontsov-Vel'yaminov (1977) of the frequency of merging events and makes it difficult to posit that bulges formed by mergers after the disks had already formed.

The Value of Simulations

Essentially two methods are available to study the merger of spiral galaxies and access the validity of the merger hypothesis. First is the systematic observation of galaxy mergers which have recently occurred the universe. As mentioned in the earlier section, mergers are short-lived phenomena and therefore rather rare, making this a difficult task. Vorontsov-Vel'yaminov (1959) and Arp (1966) have compiled catalogs of interacting and other peculiar galaxies. By studying these catalogs, one can hope to piece together the complete evolution of merger events, creating an "H-R" diagram of mergers. Unfortunately because of the relative paucity of active collisions and uncertainties in the cosmological distance scale, this task appears more difficult than that of Hertzsprung and Russell.

This thesis takes the second method, simulations, a method in the same spirit as the works of Tashpulatov (1969, 1970), and Toomre and Toomre (1972) but larger in scale by many orders of magnitude and simulating the actual physics more thoroughly and realistically. The simulations of Tashpulatov, and Toomre and Toomre contained at most a few dozen massless particles and essentially solved the restricted three-body problem for each of these particles separately. The current simulations contain on the order of 70,000 particles, divided nearly equally between luminous and dark matter, whose motion is calculated self-consistently. The magnitude of the simulations allows us to examine some of the finer structures that may be contained within

galaxy merger remnants.

Recently Barnes (1991) and Hernquist (1992) have performed simulations similar those performed for this thesis using bulgeless progenitors. They found that remnants have luminosity profiles closely resembling the $r^{1/4}$-law and scales similar to those of elliptical galaxies. Barnes found misalignment between the remnant's minor and rotation axes which constrains the process of the formation of elliptical galaxies through collisionless mergers. Furthermore, Hernquist (1992) found that the core radii of the remnants, relative their half-mass radii are much larger than those observed in real ellipticals pointing to a shortfall of the central phase-space densities of remnants relative to elliptical galaxies.

The Current Simulations

A total of thirteen simulations explored various orbital geometries and types of progenitor galaxies. Following the arguments of Binney and Tremaine (1987), we assumed the likelihood of two stars encountering each other closely to be negligible. Moreover, we neglected gas dynamics in the calculations, as the physics of the interstellar medium and especially star formation is not sufficiently understood to be reliably included in the calculations. Thus, we are left with a collisionless system of particles travelling through a relatively smooth potential.

The method

Following the discussion of Barnes (1991), such system may be

accurately described by the collisionless Boltzmann and Poison equations:

$$\frac{\partial f_k}{\partial t} + \boldsymbol{v}\cdot\frac{\partial f_k}{\partial \boldsymbol{x}} - \nabla\phi\cdot\frac{\partial f_k}{\partial \boldsymbol{v}} = 0$$
$$\nabla^2\phi = 4\pi G\int d\boldsymbol{v}(f_1 + f_2), \qquad \textbf{(1.1)}$$

where k is either 1 for the luminous matter or 2 for the dark matter. Unfortunately, it is difficult to solve these equations directly, using finite-difference methods, therefore an N-body technique is used. In essence the continuous distribution is represented by a discrete set of N_k particles for each component. These particles are given phase space coordinates ($\boldsymbol{x}_i$, $\boldsymbol{v}_i$) drawn from the appropriate phase distribution and masses $m_i = N_k^{-1}\int f_k\, d\boldsymbol{x}\, d\boldsymbol{v}$. The evolution of the phase-space is then obtained by integrating along the characteristic curves of Eq. (1.1):

$$\frac{dx_i}{dt} = v_i\,, \qquad \frac{dv_i}{dt} = -\nabla\phi|_{x=x_i} \qquad \textbf{(1.2)}$$

where the potential at each particle is approximated by

$$\phi|_{x=x_i} = -G\sum_{j\neq i}\frac{m_j}{(|\boldsymbol{x}_j - \boldsymbol{x}_i|^2 + \epsilon^2)^{1/2}}\,, \qquad \textbf{(1.3)}$$

and ε is the softening length which is introduced to smooth the potential on small scales. To return to the continuum limit, one only needs to let $N_k \to \infty$ and $\varepsilon \to 0$.

The potential at each point was calculated not by direct summation whose cost in cpu time scales as ~ $O(N^2)$ but with the "hierarchial tree" method (see Barnes and Hut 1986 for further details). In this method the potential from distant particles is approximated using low-order multipole expansions

while the effect of nearby particles is calculated using a variant on direct summation. Since the calculations may be performed on tree-structured data, the cost in cpu time scales as ~ $O(N \log N)$.

Before delving into a discussion of the initial conditions, a description of the units used throughout this thesis would be appropriate. In our system of units, G is set to equal 1 and after scaling to the Galaxy the units of length, time, and mass become respectively 3.5 kpc, 1.31×10^{7} yr, 5.6×10^{10} $M_{\odot}$. A unit velocity then corresponds to 263.3 km/sec. Each simulation was carried out through 144 time units (1.9×10^{9} yr), and the first pericenters were reached approximately 24 time units after the beginning of the simulation.

Initial conditions

As mentioned earlier, a total of thirteen simulations were performed examining a variety of initial conditions and progenitor galaxies. In essence, two types of parameters were varied. The first was the absence or presence of a bulge and whether the bulge, when present, rotated. The second was the angles of the spin axes of the progenitor galaxies with the initial orbital angular momentum of the system. The individual runs will be referred using the following system of codes (two letters, followed by two numbers): NB, OB, and RB refer to "No Bulge", "Ordinary Bulge", and "Rotating Bulge" respectively; each of the two numbers refers to one of the galaxies with 0, 1, and 2 designating that its spin axis is aligned with the orbital angular momentum, is at approximately 71° to the orbital axis, and is anti-aligned with

the orbital angular momentum respectively.

Each galaxy consisted of at least a disk and a halo. Each galaxy's disk had a mass of 1 and an exponential radial profile of surface density of scale length 1. In the vertical direction, the profile followed a sech ^{2} distribution with scale length z_0 = 0.2. Furthermore, their radial velocity dispersions were normalized so that Q = 1.5 at r = 8.5 kpc / 3.5 kpc. The halos each had a mass of 5.8. In summary, the disks and the halos followed the profiles:

$$\rho_{disk}(r,z) \propto e^{-r/r_0}\,\mathrm{sech}^2(z/z_o)$$
$$\rho_{halo}(r) \propto \frac{e^{-r/r_t}}{r^2+\gamma^2} \qquad \textbf{(1.4)}$$

where

$$r_0 = 1,\ r_t = 10,\ \text{and}\ \gamma = 1. \qquad \textbf{(1.5)}$$

In the simulations labeled OB or RB, galaxies with ordinary or rotating, oblate bulges were used as progenitors. The bulges had the following, flattened Hernquist (1990), profile:

$$\rho = \frac{M}{2\pi abcm(1+m)^3} \qquad \textbf{(1.6)}$$

where

$$m^2 = \frac{x^2}{0.2^2} + \frac{y^2}{0.2^2} + \frac{z^2}{0.1^2}. \qquad \textbf{(1.7)}$$

For the rotating bulges all the particles were forced to have the same sign of azimuthal velocity.

In each simulation the centers of mass of the galaxies were initially separated by 30 units and were given initial velocities such that they would have had followed perfectly parabolic orbits in the x-y plane with pericentric

separations of 2.5, if they acted like point masses. The choice of parabolic encounters strikes a compromise (Barnes 1991) between the highly eccentric orbits ($0 \ll e \leq 1$) of Toomre's (1977) loosely bound pairs and pairs that have been accelerated into hyperbolic orbits by a background distribution of dark matter.

Table 1.1 Encounter Parameters, Total Spin and Orbital L_z of the Luminous Matter

Run Code	i_1	ϖ_1	i_2	ϖ_2	N	Spin L_z	Total L_z	B:D:H
NB00	0		0		65536	3.5	31.6	0:3:17.4
OB00	0		0		73728	3.4	33.5	1:3:17.4
RB00	0		0		73728	3.6	33.8	1:3:17.4
NB02	0		180		65536	0.0	28.0	0:3:17.4
OB02	0		180		73728	0.0	30.1	1:3:17.4
RB02	0		180		73728	0.0	30.1	1:3:17.4
NB01	0		71	30	65536	2.5	30.5	0:3:17.4
OB01	0		71	30	73728	2.2	32.4	1:3:17.4
RB01	0		71	30	73728	2.4	32.5	1:3:17.4
NB11	71	-30	71	30	65536	1.4	29.4	0:3:17.4
OB11	71	-30	71	30	73728	1.1	31.2	1:3:17.4
RB11	71	-30	71	30	73728	1.2	31.3	1:3:17.4
NB22	180		180		65536	-2.5	24.6	0:3:17.4

Since the progenitor galaxies are axisymmetric, four angles serve to characterize the initial geometries of the encounters. The inclinations i_1 and i_2 measure the angles between the spin axes of the disks and the direction of the orbital angular momentum; thus $i = 0°$ would correspond to a galaxy rotating prograde to the orbit and $i = 180°$ to retrograde rotation. The second

pair of angles is the pericentric arguments (ϖ) which measure the angle between the line of nodes of the galaxy and the line connecting the centers of mass of the two galaxies at pericenter. Table 1.1 summarizes the geometric parameters of the 13 encounters. The values of the spin and orbital angular momenta [1] in the z direction of the luminous matter in each simulation are included to elucidate the physical effects of the varying geometry.

The following chapters explore and attempt to explain some of the observational signatures of the simulated merger remnants. Chapter 2 discusses the traces of mergers that may be betrayed by deviations of the isophotes from ellipses. In Chapter 3, the expected color gradients of mergers remnants are compared with the observed gradients in elliptical galaxies. Chapters 4 and 5 touch upon the kinematics of merger remnants: Chapter 4 discusses the distribution of velocities throughout the remnant and the connected transfer of angular momentum. Chapter 5 addresses the phase-density argument against the merger hypothesis and presents an extreme model for the role of gas in mergers to calculate the initial gas fraction needed to alleviate the phase-density problem. Finally, in Chapter 6, the investigation of the previous chapters will culminate in some conclusions concerning the merger hypothesis. An appendix outlines some recent Soviet and Russian

[1] The spin angular momentum is defined to be the angular momentum of the luminous component of each galaxy relative to its center of mass, while the orbital angular momentum describes the motion of the centers of mass of the galaxies relative to the center of mass of the system.

studies of interacting galaxies.

Bibliography

Arp, H., 1966, *Atlas of Peculiar Galaxies* (Pasadena: California Institute of Technology)

Bertola, F. and Capaccioli, M. 1975, *Ap. J.*, **200**, 439.

Carlberg, R.G. 1984, *Ap. J.*, **286**, 403-415.

Barnes, Joshua E. 1991, "Transformations of Galaxies: I. Mergers of Equal-Mass Stellar Disks" Preprint

Barnes, Josh, and Hut, Piet. 1986, *Nature*, **324**, 446-449.

Bender, R., Döbereiner, S., and Möllenhoff, C. 1987, *As. Ap. (Letters)*, **177**, L53-L56.

Bender, R., Surman, Döbereiner, S., Möllenhoff, C., and Madejsky. 1989, *As. Ap.*, **217**, 35-43.

Binney, James. 1976, *N.N.R.A.S.*, **177**, 19-29.

Binney, James. 1978, *N.N.R.A.S.*, **183**, 501-514.

Binney, J.J. and Tremaine, S. 1987, *Galactic Dynamics* (Princeton University Press)

Carlberg, R.G. 1986, *Ap. J.*, **310**, 593-596.

de Vaucouleurs, G. 1948, *Ann. d' Astrophys.* **11**, 247-287.

de Vaucouleurs, G. 1988, in *Structure and Dynamics of Elliptical Galaxies*. ed. Tim de Zeeuw (Dordrecht: D. Reidel), 3.

de Vaucouleurs, G., de Vaucouleurs, A. and Corwin, H.G. 1976, *Second Reference Catalogue of Bright Galaxies* (University of Texas Press)

Evans, David S. 1951, *M.N.R.A.S.*, **111**, 526.

Franx, Marijn, and Illingworth, Garth. 1990, *Ap. J. (Letters)*, **359**, L41-L45.

Franx, Marijn, Illingworth, Garth, and Heckman, Timothy. 1989, *Ap. J.*, **344**, 613-636.

Hernquist, L. 1990, *Ap.J.*, **356**, 359.

Hernquist, Lars. 1992, "Structure of Merger Remnants I. Bulgeless Progenitors" Preprint

Illingworth, G. 1977, *Ap. J. (Letters)*, **218**, L43.

Larson, Richard B. 1974, *M.N.R.A.S.*, **166**, 585-616.

Larson, Richard B. 1990, *P.A.S.P.*, **102**, 709-722.

Lynden-Bell, D. 1967, *M.N.R.A.S.*, **136**, 101.

Peletier, Reynier F. *et. al.* 1990, *A.J.*, **100**, 1091.

Pfleiderer, J. 1963. *Zs. f. Ap.* **58**, 12.

Pfleiderer, J. and Siedentopf, H. 1961. *Zs. f. Ap.* **51**, 201.

Rix, Hans-Walter, and White, Simon D.M.. 1992, *M.N.R.A.S.*, **254**, 389-403.

Simien, F. and Michard R. 1990, *As. Ap.*, **227**, 11-18.

Tashpulatov, N. 1969, *Astronomicheskij Zhurnal*, **46**, 1236-1246.

Tashpulatov, N. 1970, *Astronomicheskij Zhurnal*, **47**, 277-291.

Toomre, A. 1977, in *The Evolution of Galaxies and Stellar Populations*. ed. B.M. Tinsley and R.B. Larson (New Haven: Yale University Observatory), 401.

Toomre, A., and Toomre, J. 1972, *Ap. J.*, **178**, 623.

Toth, G., and Ostriker, J.P. 1992, *Ap. J.*, **389**, 5.

van Albada, T.S. 1982, *M.N.R.A.S.*, **201**, 939.

van den Bergh, S., 1990, *Q.J.R.A.S.*, **31**, 153-159.

Villumsen, J.V. 1984, *Ap. J.*, **284**, 75.

Vorontsov-Vel'yaminov, B.A. 1959, *Atlas and Catalog of Interacting Galaxies* (Moscow: Sternberg State Astronomical Institute)

Vorontsov-Vel'yaminov, B.A. 1977, *Pis'ma v Astronomicheskij Zhurnal*, **3**, 251.

Chapter 2: Isophotes

Recent advances in CCD technology have made it possible to measure the deviations of the isophotes from ellipses down to approximately two tenths of a percent. A common speculation concerning the origin of these residuals is that galaxies, which have suffered an interaction, are liable to have "boxy" isophotes while elliptical galaxies with weak disks are likely to have pointed or "disky" isophotes (Bender *et. al.* 1989). The current run of simulations gives us the opportunity to access the viability of this speculation. The isophotal contours were found for three surface brightness values from 64 different viewpoints on the thirteen simulated merger remnants, making a total of 2,498 derived isophotes. We found that on average a merger remnant appears neither "disky" nor "boxy", or in mathematical terms the mean of $a_{\cos 4\theta}$ over the various viewpoints on a given remnant is less than the standard deviation of the residual. As a side benefit of the isophote derivation, we calculated the ellipticities of each of these isophotes and examined their distribution.

The Predictions

In a prograde-prograde collision of two disks (the spins of both disks are pointing in the same direction as the orbital angular momentum), one would initially expect the remnant to appear boxy from viewpoints directly above and below the plane of the orbit, because the dense central region of the remnants are dominated by radial or box orbits. However, from most viewpoints near the plane of the orbit, one would expect to see the remnant of the disks of

progenitor galaxies, creating pointed or disky isophotes. Indeed in the more symmetric of the simulations, NB00, (see Chapter 1 for an explanation of these codes), this effect is manifest; however, with more complicated initial conditions, the boxy-disky question is more elusive.

The sixty-four viewpoints from which each merger remnant is viewed, were uniformly distributed over the quadrant of the sphere with $y > 0$ and $z > 0$. Figure 2.1 depicts the location of the viewpoints on the unit sphere. The viewpoints were selected from only this quadrant to take advantage of the symmetries of most of the encounters. One cannot expect that these symmetries will be preserved for the runs that begin with both galaxies' spin axes pointing askew of the orbital angular momentum vector; however, for the isophotal analysis it is still a good, time-saving assumption.

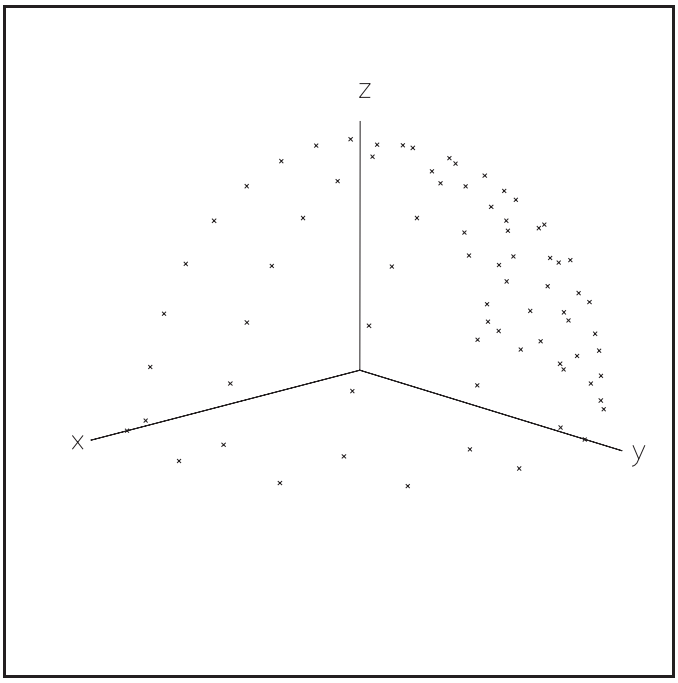

Figure 2.1 Viewpoints for Isophote Analysis

For each orientation, the distribution of luminous particles in the merger remnant were projected onto a plane; all the particles outside a square with sides 20 units long, centered on the projection of the origin were discarded in

the analysis. This 20-by-20 square was translated into a 200-by-200 pixel image, and the value of each pixel was the number of particles projected within the boundaries of that pixel. Next, for use with image processing software, the counts in each image were scaled linearly onto the range 0 to 32,767. Finally, the images were smoothed with a two-dimensional Gaussian with a FWHM equal to 2.4 pixels or a deviation of one pixel. The final smoothing served to reduce the noise that the discreteness of the N-body simulation produced.

Finding the isophotes

For each viewpoint, three goal isophotal levels were selected at 4.6%, 3.1% and 1.5% of the peak pixel value for that orientation; these percentages correspond to 1500, 1000, and 500 counts after the images had been scaled such that the maximum value in the image was 32,767. These levels correspond to the outer regions of the remnants where in general the deviations of the isophotes from ellipses was the strongest. At each of these levels, an isophote was found through a non-linear least squares fit. The first step was to find the center of brightness of the image, given by the following equation:

$$x_{Center} = \frac{\sum_{i,j} x_{i,j} B_{i,j}}{\sum_{i,j} B_{i,j}} \text{ and } y_{Center} = \frac{\sum_{i,j} y_{i,j} B_{i,j}}{\sum_{i,j} B_{i,j}}. \qquad \textbf{(2.1)}$$

where $B_{i,j}$ is the value of the ith pixel in the jth row. To simplify and speed the fitting process, this center of brightness was taken to be the center of the isophotes. Next, the algorithm minimized

$$X^2 = \frac{\sum W_{i,j}(B_{i,j} - goal\ level)^2}{\sum W_{i,j}} \qquad \textbf{(2.2)}$$

over the entire image, where $W_{i,j}$ is a weighting function which ranges from one if the pixel *(i,j)* is directly on top of the current guess isophote to zero if the pixel is outside a range of four pixels from the guess isophote. The customary least-squares sum was divided by the sum of the weights to prevent isophote bins with small areas from getting disproportionately small X^2 values. $W_{i,j}$ is given by the following equation

$$W_{i,j} = \begin{cases} 1 - \left(\frac{r_{i,j} - r(\theta_{i,j})}{4}\right)^2 & \text{if } |r_{i,j} - r(\theta_{i,j})| < 4 \\ 0 & \text{otherwise} \end{cases} \qquad \textbf{(2.3)}$$

where $r_{i,j}$ is the distance of the pixel from the center and $r(\theta)$ is the equation of the current guess isophote in polar coordinates. To speed the process, the routine found the circles inscribing and circumscribing the region where $W_{i,j}$ is non-zero and only calculated X^2 for the pixels within the region between these two circles. The equation of the isophote in polar coordinates ($r(\theta)$) in all its grandeur is

$$r(\theta) = a\left(\frac{1}{\sqrt{1-(r^2+1)\cos^2(\theta - \theta_0)}} + \zeta_{cos4\theta}\cos\left[4(\theta - \theta_0)\right]\right) \qquad \textbf{(2.4)}$$

where a, r, θ_0 are a semiaxis, the aspect ratio, and the position angle of the underlying ellipse, and $\zeta_{cos4\theta}$ is the residual fourth-order harmonic of the isophote. Since r was not constrained to be less than one during the minimization, a is simply the length of one axis of ellipse and ra is the length of the other. The residual of sin 4θ was neglected in the analysis under the

assumption that any underlying disk or box would coincide with the axes of the ellipse.

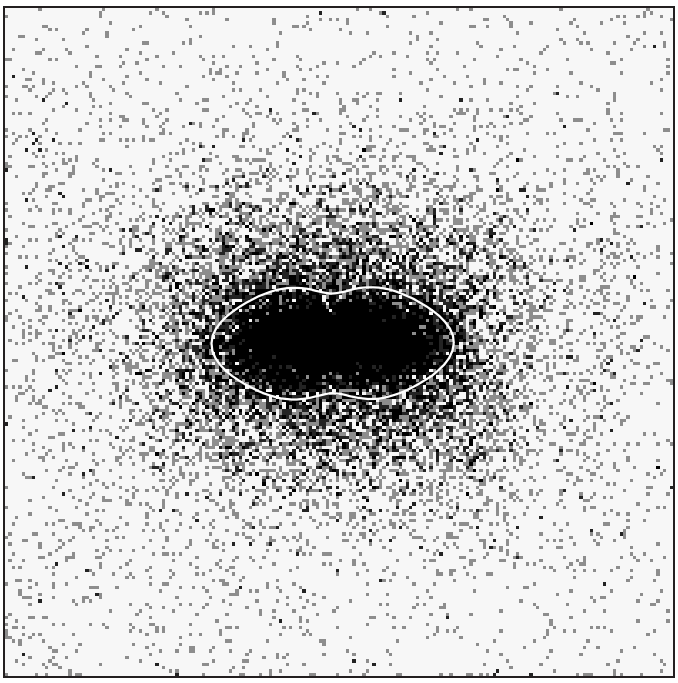

Figure 2.2 Isophote of NB00 at 1000 counts

The minimization was performed in three steps. During the first step, the parameter $\zeta_{\cos 4\theta}$ was fixed to be zero, and an elliptical isophote was fitted to the image. In the second step, $\zeta_{\cos 4\theta}$ was allowed to vary with the ellipse fixed, and finally in the third step, all the parameters were freed to find the best-fitting isophote. The process was carried out in the three steps to assure that the minimization routine was given reasonable initial conditions for the final fit. In the end, these added precautions probably did not slow the algorithm much.

To estimate the errors of the algorithm, the isophotes were fitted on two sets of test images with known ellipticities and fourth-order residuals. A total of 200 exponential profiles were generated. In the first set, their ellipticities ranged from 0 to 0.7 and their $\zeta_{\cos 4\theta}$ residuals ranged from -0.1 to 0.1. Then the routine fit isophotes to these images, and its results could be compared with the actual values. The root-mean-squared errors in radius, aspect ratio,

position angle, and the residual were 0.11, 0.0037, 0.54°, and 0.016 respectively. More importantly, the root-mean-squared fractional errors were 0.62%, 0.63% and 54% for the radius, aspect ratio, and residual. A second series of Monte-Carlo runs was performed with $\zeta_{\cos 4\theta}$ ranging from -0.03 to 0.03. As expected, the errors in determination of radius, aspect ratio and position angle were comparable to those in the first run. However, the error in the residual decreased in an absolute sense to 4.7×10^{-3} and increased to a fractional error of 123%. Since the measured $\zeta_{\cos 4\theta}$ of the merger remnants are in general well contained within the range -0.03 to 0.03, the uncertainties in residual determination will be taken to be 4.7×10^{-3} in both directions. This error in the measurement of the residual is a bit larger than the errors estimated by Bender *et. al.* (1987), Franx (1988), and Michard and Simien (1988) - approximately 2×10^{-3} to reduce observational data. A possible reason for this is that these researchers could sample the images more finely than in the current investigation. In our study, a finer sampling either through decreasing the width of the trial isophotal bin or increasing the total number of pixels would allow the discreteness of the N-body simulation to play a deciding role. Regardless, as will be seen in the following sections, the $\zeta_{\cos 4\theta}$ derived from the images usually exceeded this estimated error.

A second set of Monte-Carlo simulations were performed to determine how the errors would scale with an increase in particle number. Isophotes were fit to 50 400-by-400 test images which would have the same level of

counting errors if the number of luminous particles were increased by a factor of four. This second analysis determined that the error in isophote derivation scales inversely with the square root of the number of luminous particles in the simulation. Thus, an increase of the number of particles by a factor of four would bring the errors on this routine within the range of errors estimated for the observations.

Figure 2.2 depicts the results of the algorithm for the isophote at 1,000 counts on an image of NB00 viewed from near the z-axis. As predicted in the preceding section, from this viewpoint NB00 does have boxy and rather flattened isophotes. The parameters for the isophote depicted are

$$a = 16.5,\ r = 0.436,\ \theta_0 = 0.4°,\ \text{and}\ \zeta_{cos4\theta} = -0.0939. \qquad \textbf{(2.5)}$$

The minimum of X^2 for this fit was 47.6. For the set of 200-by-200, Monte-Carlo images the mean value of X^2 was approximately 6. Considering that the Monte-Carlo images had "perfect" isophotes, a value of X^2 of 47.6 represents a good fit to the noisier images of the remnants.

Distribution of ellipticities

When examining the ellipticities of the merger remnants as a function of the initial conditions and isophote level in Table 2.1, a few trends are evident. First, for a given set of initial conditions, the ellipticity of the isophotes changed little with changes in isophote level or equivalently radius from the center. On the other hand, the initial conditions play a strong role in determining the average ellipticity of the remnant. Intuitively, one would expect that the presence of a relatively spherical luminous components would

Table 2.1 Ellipticities - Means and Dispersions

Run Code	Level = 500		Level = 1000		Level = 1500	
	Mean	σ	Mean	σ	Mean	σ
NB00	0.52	0.18	0.57	0.14	0.58	0.14
OB00	0.41	0.18	0.39	0.16	0.39	0.15
RB00	0.39	0.20	0.39	0.17	0.38	0.16
NB02	0.47	0.21	0.47	0.19	0.48	0.17
OB02	0.41	0.20	0.41	0.18	0.40	0.18
RB02	0.42	0.20	0.42	0.19	0.42	0.16
NB01	0.34	0.10	0.35	0.09	0.36	0.10
OB01	0.30	0.09	0.33	0.09	0.35	0.10
RB01	0.30	0.09	0.32	0.09	0.34	0.09
NB11	0.36	0.10	0.38	0.10	0.38	0.10
OB11	0.29	0.14	0.31	0.13	0.32	0.12
RB11	0.27	0.13	0.29	0.12	0.31	0.11
NB22	0.45	0.23	0.43	0.22	0.43	0.22

decrease the ellipticity of the remnant, and just this effect is seen.

The second effect is a little more difficult to explain, but is no weaker. The initial conditions all effectively define at least one preferred plane, the orbital plane. As this preference is weakened by contradicting conditions, the ellipticity of the remnant decreases. The inclination of the disk is probably the most important factor. The initial presence of luminous matter outside of the orbital plane as expected increases the amount of material outside the plane after the merger and thus decreases the ellipticity. Some additional factors are the spin angular momenta of the various components. A spin anti-aligned with

the orbital angular momenta effectively weakens the preference toward the orbital plane. However, even stronger is the effect of a skew spin which defines another preferred plane. These secondary effects are noticeable when comparing run NB00 with NB02 and NB22, or run OB11 with RB11. In the first comparison, the counterrotation of the disk weakens the preference toward the orbital plane. And in the second, the rotation of the bulges strengths the preference toward the two planes of the disks of the galaxies.

By this rule of thumb, one would expect the most spherical remnants to come from encounters with the both disks inclined to the orbital plane and their spins pointing away from the direction of the orbital angular momentum. Also, one would expect that in the case of multiple collisions, with each new merger a preference toward any one plane would weaken and the ellipticity of the product would decrease.

By examining the variation of ellipticity with viewpoint, in effect one studies indirectly the three-dimensional structure of the remnant. Although we have direct access to the actual three-dimensional distribution of matter, observers do not have this luxury, but rather they must statistically average over many galaxies to get an idea of their three-dimensional structure.

In the axisymmetric case, there are two extremes: the sphere and the thin, planar disk. The sphere, when observed from any angle, would appear circular ($e = 0$). The ellipticity of the planar disk, on the other hand, would be a function of the inclination (i) of the disk relative to the line of sight ($e = 1 -$

sin i) where $i = 0°$ is edge-on and $i = 90°$ is face-on. This slight digression will help to explain to the role of the abscissa in Figure 2.5 and Figure 2.4. Because the viewpoints were selected uniformly over the unit sphere, the number of the viewpoint is proportional to 1 - sin i, as depicted in Figure 2.3. Here i is the inclination of the orbital plane to the line of sight. The first viewpoint has $i \approx 90°$ and the sixty-fourth, $i \approx 0°$. Therefore, a thin disk in the orbital plane would appear as a series of lengthening steps whose height would increase linearly with the viewpoint number.

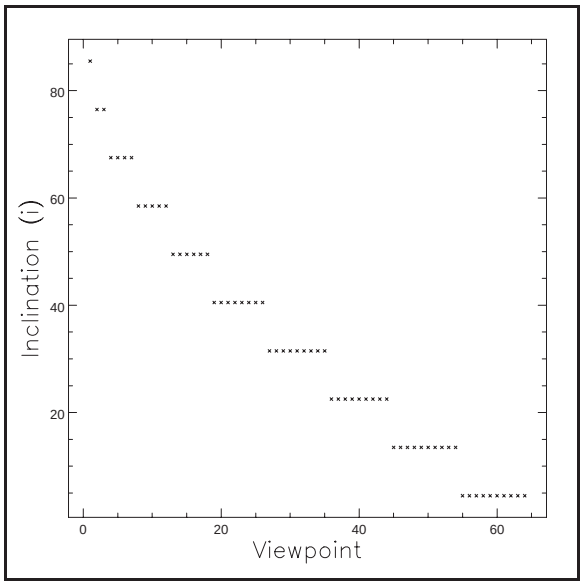

Figure 2.3 Inclination Angle as a Function of Viewpoint Number

Figure 2.4 essentially shows this dependence. If we ignore the high frequency fluctuations which are due to changes in azimuth (the merger remnant is not axisymmetric after all), there is a linear dependence of ellipticity on the viewpoint number, indicating that one can, to a rough first order, model remnant NB00 as a thin disk in the original orbital plane. Figure 2.5 which depicts the relationship for RB11 tells a quite different story. The ellipticity actually decreases slightly with the viewpoint number, and the high-frequency (azimuthal) variation is much stronger than in

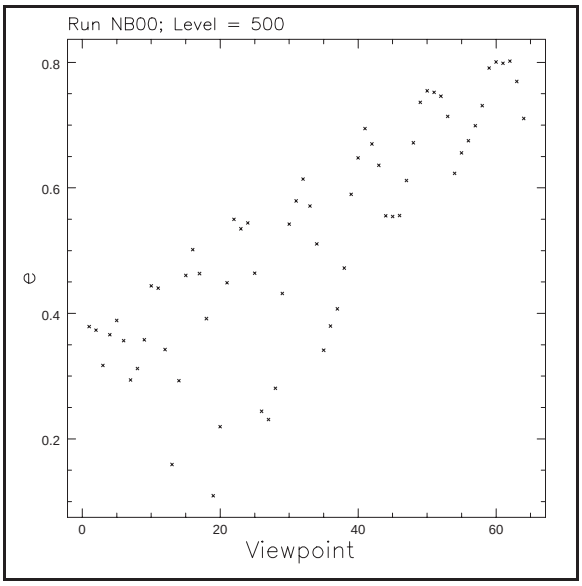

Figure 2.4 Ellipticity versus Viewing Angle

Figure 2.4. These two signs indicate that remnant RB11 may be more spherical than NB00, and more definitely that our choice of the initial orbital plane as the plane of the galaxy was misguided.

Distribution of "boxiness"

The measurements of the "boxiness" as expected from the error analysis described above were less telling. The distributions of $\zeta_{\cos 4\theta}$ in most of the remnants are consistent with a mean $\zeta_{\cos 4\theta}$ of zero over the orientations with a spread largely caused by measurement error given the larger error estimate of 0.016. To examine the distributions further, we will adopt the smaller error estimate of 4.7×10^{-3}, although it may be an underestimate. An examination of Table 2.2 reveals that for the majority of remnants the mean value $\zeta_{\cos 4\theta}$ differs from zero by only a few times 2×10^{-3}, the formal error quoted by Bender *et. al.* (1987), Franx (1988), and Michard

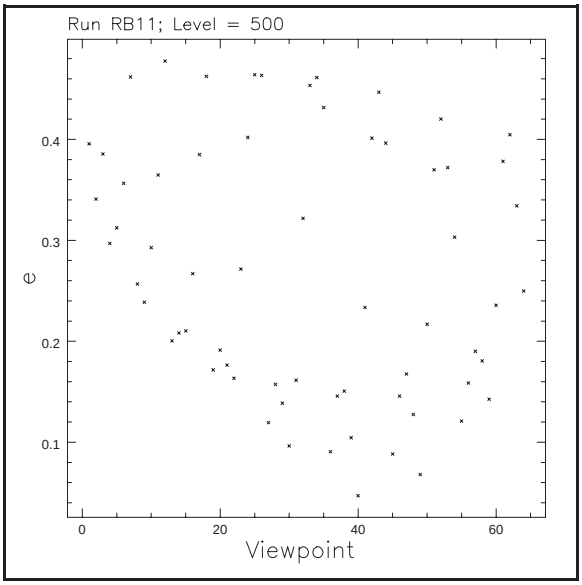

Figure 2.5 Ellipticity versus Viewing Angle

Table 2.2 $\zeta_{\cos 4\theta}$ - Means and Dispersions

Run Code	Level = 500		Level = 1000		Level = 1500	
	Mean	σ	Mean	σ	Mean	σ
NB00	-0.029	0.037	-0.042	0.042	-0.027	0.033
OB00	-0.003	0.012	-0.004	0.011	-0.004	0.013
RB00	-0.001	0.013	-0.004	0.014	-0.003	0.014
NB02	-0.002	0.029	-0.003	0.022	-0.001	0.019
OB02	-0.003	0.010	-0.001	0.013	-0.004	0.017
RB02	-0.004	0.010	-0.006	0.014	-0.008	0.018
NB01	0.002	0.027	-0.002	0.013	-0.006	0.009
OB01	-0.007	0.011	-0.007	0.011	-0.008	0.015
RB01	-0.007	0.010	-0.011	0.012	-0.010	0.013
NB11	0.017	0.037	0.021	0.037	0.016	0.026
OB11	-0.003	0.013	-0.002	0.011	-0.003	0.011
RB11	0.029	0.008	-0.001	0.007	-0.001	0.010
NB22	-0.004	0.024	-0.002	0.014	0.000	0.017

and Simien (1988). Furthermore, the dispersions in the measurements of $\zeta_{\cos 4\theta}$ are of the order of or larger than the mean values for all model remnants. These two observations indicate that it is not appropriate to say that merger remnants are in general "disky" or "boxy", but rather the observed deviations from ellipticity are a strong function of viewing angle and initial conditions.

As in the section on ellipticity, it is useful to examine the most (NB00) and least symmetric (RB11) cases more thoroughly. Figure 2.6 depicts the relative distribution over viewpoint of the fourth-order residuals of the 1000-

count isophotes for the NB00 model. As can be seen in the figure, the distribution of $\zeta_{\cos 4\theta}$ is strongly skewed toward negative or "boxy" values. The earlier discussion foreshadowed this result. For the symmetric encounter, the box orbits of the dense central region cause the appearance of boxy isophotes when the object is seen from above or from certain viewpoints in the orbital plane. The relationship of $\zeta_{\cos 4\theta}$ versus viewpoint number shown in Figure 2.7 supports this argument; the isophotes on average go from being boxy to disky as the viewpoint moves closer to the orbital plane.

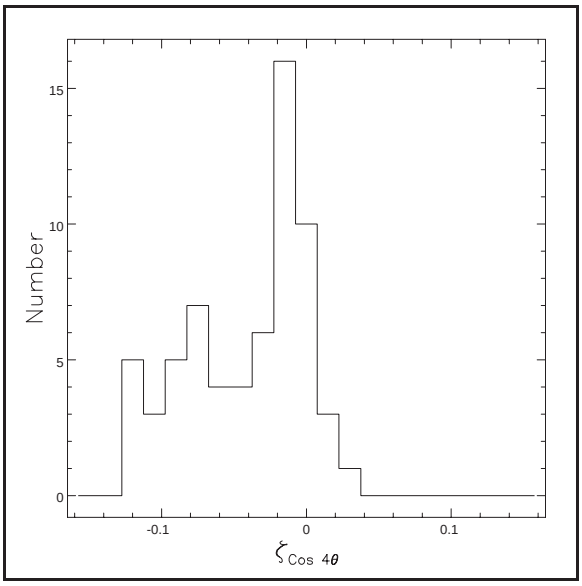

Figure 2.6 Distribution of $\zeta_{\cos 4\theta}$

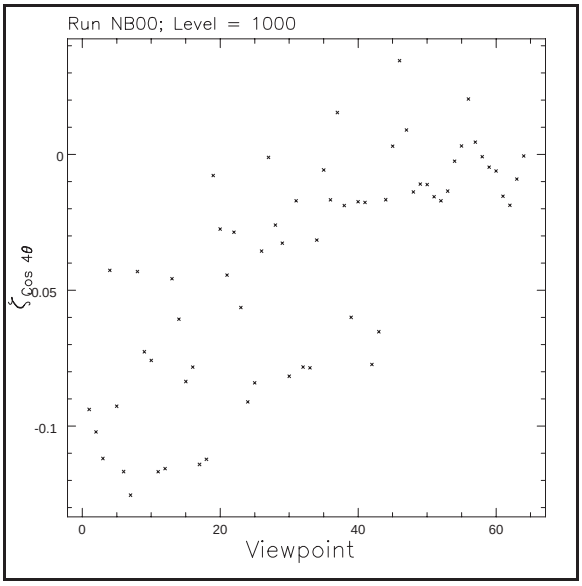

Figure 2.7 $\zeta_{\cos 4\theta}$ versus Viewing Angle

The picture for the model RB11, as expected, is a bit less clear. Figure 2.9 shows the distribution of $\zeta_{\cos 4\theta}$ for RB11, again for the isophotes at 1,000 counts (the scale in Figure 2.9 is five times finer than in Figure 2.6). The dispersion in $\zeta_{\cos 4\theta}$ may be caused entirely by measurement errors. The

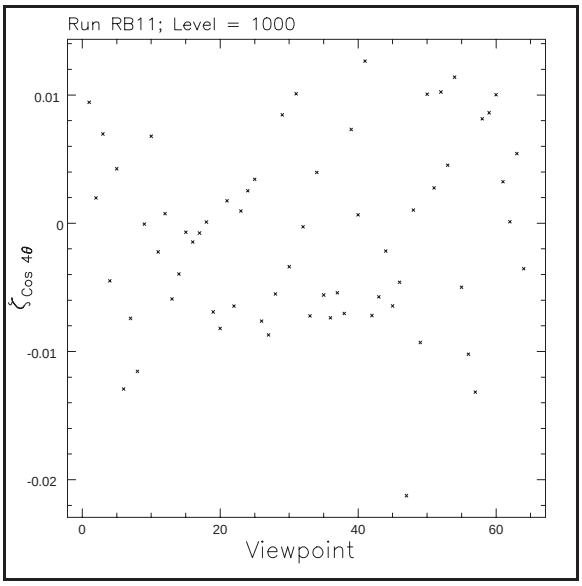

Figure 2.8 $\zeta_{\cos 4\theta}$ versus Viewing Angle

dependence of $\zeta_{\cos 4\theta}$ on the viewing angle, as depicted in Figure 2.8, is weak if it exists at all.

The Observations

With the use of CCDs, recent observations of ellipticals have been able examine the question of how the isophotes of elliptical galaxies deviate from perfect ellipses. Franx (1988) noticed strong cos 4θ (greater than 1.0%) deviations in few of the 17 ellipticals he observed. Furthermore, he found that in agreement with the results here, that the sign as well as the absolute value of the residual may be a function of viewing angle. Michard and Simien (1988) presented a more extensive analysis of the isophotes of ellipticals. Out of the eighteen ellipticals observed, two had boxy isophotes all at radii measured, four had only disky isophotes, while the remaining twelve ellipticals switched from being boxy to disky or vice versa and sometimes more

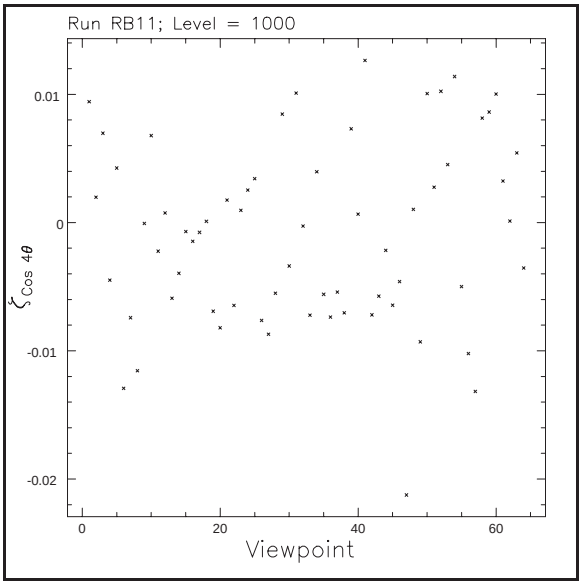

Figure 2.9 Distribution of $\zeta_{\cos 4\theta}$

than once.

The work of Bender and his collaborators may represent the most extensive study of these features of elliptical galaxies. They found from a magnitude-limited sample of northern ellipticals (Bender *et. al.* 1989) that ~ 1/3 show boxy isophotes, ~ 1/3 disky, and ~ 1/3 have isophotes which change from disky to boxy or vice versa. Furthermore, they found that the presence of radio or x-ray activity (Bender *et. al.* 1987; Bender *et. al.* 1989) is correlated with boxy isophotes and their absence with disky isophotes, and that galaxies with pointed isophotes resemble S0 galaxies by containing rotationally supported disk components (Bender 1988). Thus, they posit that "it seems to be evident that boxy and disky ellipticals represent different tracks of galaxy evolution (Bender *et. al.* 1989).

Reconciliation

The isophote analysis of the thirteen model merger remnants leads to us make a few conclusions about the merger hypothesis. First, that within the errors of the fitting algorithm mergers simulated which only sample a small portion of the space of initial conditions produce boxy and disky in approximately equal numbers. Within the limits of the simulations, the formation of ellipticals through mergers does not discriminate on the basis of boxiness or diskiness, and cannot provide a "different track of galaxy evolution" for disky versus boxy ellipticals. Second, Bender *et. al.* (1989) claim that the sign of the deviation from elliptical isophotes (*i.e.* whether the galaxy is disky

or boxy) is not a function of viewing angle. On the basis of this analysis, we must disagree with this assumption and side with the Franx's opposing claim (1988). It turns out that the predictions of the merger hypothesis as far as isophotes are concerned are much more complicated and subtle than diskiness or boxiness.

Bibliography

Bender, R. 1988, *As. Ap. (Letters)*, **193**, L7-10.

Bender, R., Döbereiner, S., and Möllenhoff, C. 1987, *As. Ap. (Letters)*, **177**, L53-L56.

Bender, R. and Möllenhoff, C. 1987, *As. Ap.*, **177**, 71-83.

Bender, R., Surman, Döbereiner, S., Möllenhoff, C., and Madejsky. 1989, *As. Ap.*, **217**, 35-43.

Franx, Marijn. 1988, *Structure and Kinematics of Elliptical Galaxies*, PhD Thesis.

Michard, R. and Simien F. 1988, *As. Ap. Suppl.*, **74**, 25-51.

Simien, F. and Michard R. 1990, *As. Ap.*, **227**, 11-18.

Chapter 3: Color Gradients in Merger Remnants

The origin of the color gradients in elliptical galaxies has long been a question of much speculation. Gradients in metallicity are formed quite naturally in simulations of the dissipative formation of elliptical galaxies (Larson 1970; Carlberg 1984), as metal-enriched gas from the earlier generation of stars sinks to the center of the potential. Thus a gradient of decreasing metallicity with radius appears and assuming that color is a well-defined function of metallicity, a color gradient forms as well. Franx and Illingworth (1990) describe a complementary process without dissipation in which outward-flowing winds driven by supernovae produce a correlation between color and local escape velocity.

In mergers without large quantities of gas, or equivalently under the condition that the merger causes a negligible amount of star formation), the metallicities of individual stars cannot change appreciably. Thus, the color gradients in the youngest remnants can only depend on the gradients in the progenitor galaxies and the violence of the interaction, because stars of each range of color will follow the collisionless Boltzmann equation separately under the influence of the same potential (Binney and Tremaine 1987). Thus the problem of color gradients can be reduced to a question of how mergers map stars at a given position in the progenitor galaxies to another position in the remnant. By pulling the rug over the question of star formation, a few additional problems are uncovered.

First, we have to understand the initial color gradients in spiral galaxies especially including the bulge. Although much work has studied the gradients in the disks of spiral galaxies, the bulges have been much less accessible due to observational constraints. Second, we have to understand the dynamics of the mapping in configuration space from the progenitor galaxies to the remnant, and how this mapping is affected by the geometry of the collision. Here the simulations are indispensable.

Some Predictions

The merger of two galaxies may result in color gradients profoundly different from those in the remnant, if either phase mixing or gas dynamics is important during or after the merger. The magnitude of the first effect may easily be estimated by studying the simulations; to understand the second effect is more difficult, even though it may play a more important role.

Phase mixing

Although the collisionless Boltzmann equation maps patches of phase space onto patches of the same volume, generally it will not map these patches into regions of the same or even similar shape (see Binney and Tremaine 1987 for a discussion of phase mixing). Therefore the merging process can stretch an initially compact region in radius over large range in radius and mix particles from other radial regions into the region under examination; consequently, if violent relaxation is efficient, one would expect a merger to weaken and even erase an initial color gradient. Fortunately, it is not.

Figure 3.1 depicts how luminous particles at various initial radii from the center of their component are mapped to final radii from the center of the remnant. The simulation depicted is NB00, the most symmetric of the encounters and as it turns out the most violent in terms of erasing color gradients.

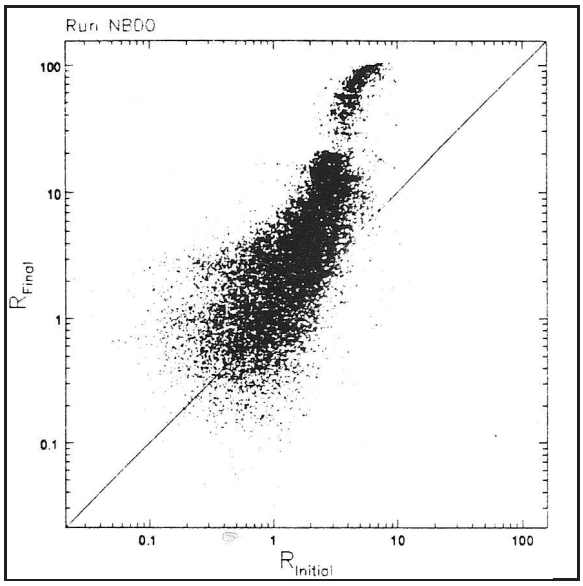

Figure 3.1 R_{Final} vs. $R_{Initial}$: Run NB00

We notice that although the spread in final radii for a given initial radii is appreciable, the correlation between initial and final radius is strong. Furthermore, a small range in initial radii is mapped onto a larger range of final radii which leads us to expect that color gradients would be weakened during the merger. For comparison, Figure 3.2 depicts the mapping for the least symmetric run, RB11. The two mappings differ little except that the particles in RB11 span a larger range in initial radius down to approximately 0.01. Not unexpectedly, the remnant RB11 has more particles near the center than NB00 which may affect the final color gradient of the model. Otherwise the mappings are nearly identical.

After the merger

Following the merger, the principal question is what happens to the gas in the progenitor galaxies. Two effects are important. First, young, bright

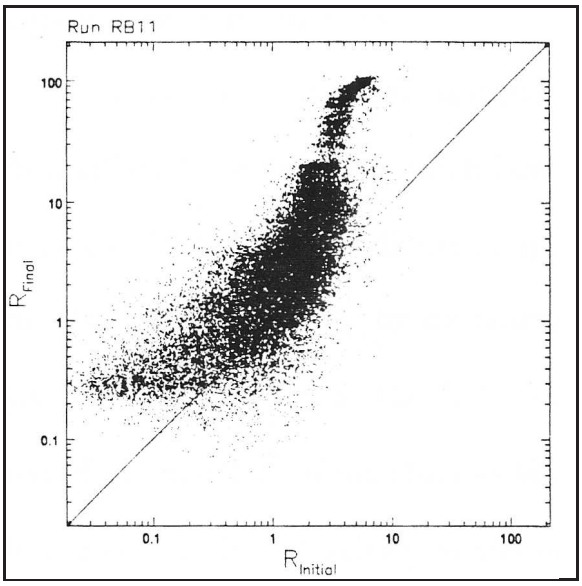

Figure 3.2 R_{Final} vs. $R_{Initial}$: Run RB11

stars determine the initial color gradient as described in the following section at large radii. After the collision, even if the gas in retained by the remnant, simulations show that the gas flows to the center and fuels star formation there rather than at large radii (Barnes and Hernquist 1990); consequently, the blue stars that will dominate the outer regions of the remnant will soon die without new stars being born there, and the outer regions will become redder. Meanwhile, at the center a new generation of stars will be born with bright, young, blue stars dominating the light at first. Thus, the distribution of initial star formation will decrease the gradient predicted by our stellar dynamical model. However, there is a second effect; after the O and B stars of the first post-merger generation die off, the more long-lived, redder stars will dominate the light at the center. Furthermore, these stars will have a higher metallicity than the stars dominating the light in the outer regions and therefore will in general be redder. The following discussion neglects these competing effects to simplify the analysis and focuses on answering the question whether the observed color gradients in elliptical galaxies can be produced by dissipationless mergers.

Initial Color Gradients

Although by using metallicity gradients we could possibly sidestep the first effect, the discussion will follow the color gradients instead for variety of reasons. Metallicity gradients in spiral disks are available (*e.g.*, Garnett and Shields 1987 for M101) by measuring the metal abundances in HII regions. However, this measures the metal richness of the gas and the youngest stars, not of the majority of the stars in the system. Second, these gradients are all but unavailable for spiral bulges other than that of Milky Way. Finally, although metallicity gradients in ellipticals have recently been measured (Schweizer *et. al.* 1990; Boronson and Thompson 1991; Couture and Hardy 1990), the color gradients in these systems have been studied and analyzed more thoroughly and in more galaxies.

The Andromeda model

The progenitor galaxies were loose models of the Milky Way, but unfortunately data on color gradients of the galactic bulge and disk, especially as viewed from outside, are not available; therefore, we tried for the next best thing. Using Sandage, Becklin and Neugebauer's (1969) photometry of Andromeda's bulge and Walterbos' (1986) data concerning its disk, we created a model of the *U-B* colors over the progenitor galaxy. We fitted a Gaussian to the measurements of Andromeda's bulge, while a linear fit sufficed for the disk.

Particles in the bulges of the progenitors were assigned a color by the

formula:

$$U-B = 0.1929\,e^{-Q^2/\lambda^2} + 0.5875 \tag{3.1}$$

where

$$Q^2 = 4z^2 + r^2 \text{ and } \lambda = 0.02506, \tag{3.2}$$

and disk particles were assigned a color using the formula,

$$U-B = -\frac{r}{15.74} + 0.5450. \tag{3.3}$$

In the preceding formulae, r is the distance of the particle from the rotation axis, and z is the height above the plane of the disk, both in dimensionless units. Therefore, the disk has a purely radial gradient, and the color of the bulge is constant on oblate ellipsoids.

The Results of the Simulations

We analyzed the color gradients in the merger remnants in three ways. First, a second-degree polynomial was fit to the U - B color along the major axis of the remnant in projection to estimate the radial gradient. Second, in the spirit of the analyses of Peletier *et. al.* (1990) and Franx *et. al.* (1989), a linear function of the logarithm of the radius was fit to U - B along the major axis. And third, to compare with the analysis of Franx and Illingworth (1990), we examined the relationship between U - B and local escape velocity.

The analysis of the previous chapter on isophotes assisted in the reduction of this section. Each remnant was "observed" from the same 64 viewing positions and at the same resolution as in the previous section; however, in this analysis the mean color of each pixel was calculated. Furthermore, for each orientation, the major axis derived by the isophote

routine at 1,000 counts was used as the major axis of this analysis. Finally the pixels were binned in radius in a stripe eight pixels wide centered upon the major axis. Thus, the color as a function of radius was measured for each orientation of each remnant.

Table 3.1 Linear *U - B* Gradients

Run Code	R_c (kpc)	d(U - B)/Dr 10^{-4} (kpc^{-1})		d(U - B)/d(R/R_c) 10^{-4}		d^2(U - B)/Dr^2 10^{-6} (kpc^{-2})	
		Mean	σ	Mean	σ	Mean	σ
NB00	1.29	-8.2	3.1	-10.5	4.0	3.0	4.1
OB00	0.64	-22.7	3.0	-14.5	1.9	22.1	4.8
RB00	0.93	-17.0	3.5	-15.8	3.3	11.8	11.8
NB02	2.56	-8.1	3.3	-20.8	8.4	-0.3	5.0
OB02	2.39	-14.2	5.0	-33.8	11.8	7.3	8.1
RB02	2.44	-14.7	4.7	-35.9	11.5	8.9	6.7
NB01	2.31	-6.7	3.5	-15.5	8.2	-4.7	5.0
OB01	2.62	-13.0	3.8	-34.2	10.1	5.5	6.3
RB01	2.64	-13.2	4.4	-34.8	11.7	5.8	7.7
NB11	1.19	-7.4	2.8	-8.8	3.3	-0.9	5.0
OB11	0.90	-18.5	4.0	-16.6	3.5	13.4	5.3
RB11	1.00	-18.6	2.9	-18.6	2.9	11.8	5.8
NB22	1.46	-10.1	2.6	-14.7	3.8	0.8	4.8

The *U - B* color as a function of radius was fit to both a second degree polynomial and to a logarithmic function in radius. The two models were of the form:

$$U-B = (U-B)_0 + \left\langle \frac{d(U-B)}{dr} \right\rangle r + \frac{1}{2}\left\langle \frac{d^2(U-B)}{dr^2} \right\rangle r^2 \qquad \textbf{(3.4)}$$
$$U-B = (U-B)_{\log,0} + \left\langle \frac{d(U-B)}{d\log r} \right\rangle \log r .$$

The results of the first analysis are presented in Table 3.1; the gradients are also presented with respect to R/R_c where R_c is the core radius of the best fitting three-dimensional Hubble profile to the particular remnant. For the fitting procedure, the remnant was assumed to be spherically symmetric; therefore, R_c should be taken only as a estimate of the linear scale of the remnant. A three-dimensional Hubble profile was used over a series of two-dimensional fits for each projection mainly to save computational effort and to reduce the effect of counting noise on the fit.

Two distinct trends are noticeable. The presence of a bulge in the progenitors steepens the color gradient substantially. This is not surprising, as the bulge of the progenitor galaxies were assigned rather steep initial color gradients (see Eq. (3.1)). The second effect is revealed when comparing the color gradient versus scale length for different geometries. The runs NB00 and RB00 stand out as having the most shallow color gradients. These geometries appear to most effectively mix the particles in radius, therefore weaken the color gradient. Concerning the second derivatives with respect to radius, this parameter seems to play a less striking role once it is averaged over orientations. For most of the models the dispersion in this parameter is of the order of its value or greater.

Table 3.2 presents the results of the logarithmic fits. Again as with the linear fit, the bulgeless models have shallower gradients than those with bulges. The second trend is not noticeable in the analysis. However, the runs RB02 and RB01 do seem to most effectively weaken the initial color gradient, as measured in this manner.

Table 3.2 Logarithmic *U - B* Gradients

Run Code	d(U-B)/d(log r) 10^{-2}	
	Mean	σ
NB00	-1.45	0.42
OB00	-3.44	0.30
RB00	-3.16	0.61
NB02	-1.64	0.41
OB02	-2.65	0.72
RB02	-2.69	0.78
NB01	-1.42	0.39
OB01	-2.33	0.50
RB01	-2.47	0.53
NB11	-1.42	0.36
OB11	-3.27	0.63
RB11	-3.37	0.52
NB22	-1.72	0.42

For the analysis *á la* Franx and Illingworth (1990), the potential of each particle was used to calculate its escape velocity. Then the particles were placed into bins 100 km/sec wide from 0 to 1000 km/sec using the escape velocity. For each bin, the mean and dispersion of the color was calculated. A result of this calculation is presented in Figure 3.3. The results of the fits for all thirteen simulations are presented in Table 3.3.

The Observations

Peletier *et. al.* (1990) and Franx *et. al.* (1989) have studied the color gradients in ellipticals in the *U, B,* and *R* bands. They give their results in the form of logarithmic gradients in *B-R* and *U-R* from which we calculated the *U-*

B gradients, in a form similar to that of Table 3.2. The results of these two investigations are presented in Table 3.4. When the values of the logarithmic gradients in the simulated merger remnants are compared with the mean observed gradient of -0.14, it is obvious that

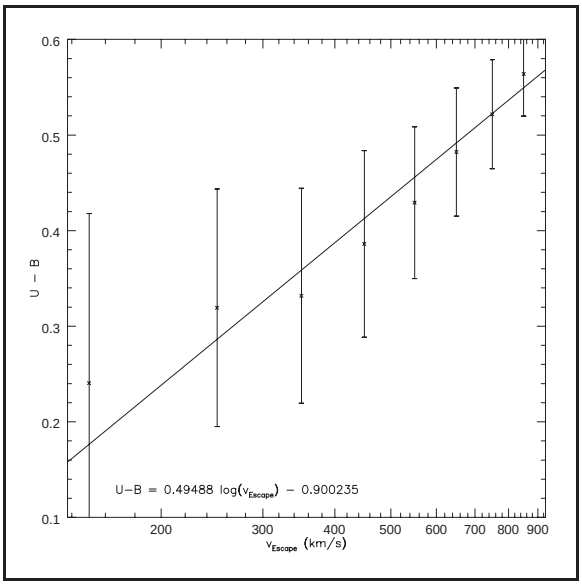

Figure 3.3 *U - B* vs. V_{esc}: Run RB11

Table 3.3 Gradient of *U - B* vs. V_{esc}

Run Code	d(U-B)/d(log v_{esc})	Run Code	d(U-B)/d(log v_{esc})
NB00	0.422	NB01	0.444
OB00	0.423	OB01	0.445
RB00	0.421	RB01	0.446
NB02	0.437	NB11	0.500
OB02	0.435	OB11	0.492
RB02	0.440	RB11	0.495
		NB22	0.541

mergers fall short by a factor of a few from reproducing the logarithmic gradients. On the other hand, like many problems in astrophysics, a factor of a few may be close enough to merit further attention.

Franx and Illingworth (1990) have attempted to determine if the color in an elliptical galaxy is a function of the local potential or escape velocity

Table 3.4 Observed Logarithmic Gradients

Galaxy	Mean	±	S	Galaxy	Mean	±	S
NGC 636	-0.17	0.08	F	NGC 3605	-0.06	0.04	P
NGC 1379	-0.06	0.25	F	NGC 3665	-0.04	0.04	P
NGC 1395	-0.22	0.08	F	NGC 3801	-0.38	0.18	P
NGC 1399	-0.08	0.21	F	NGC 4261	-0.16	0.06	P
NGC 1404	-0.07	0.05	F	NGC 4278	-0.25	0.05	P
NGC 1407	-0.10	0.18	F	NGC 4374	-0.17	0.02	P
NGC 1439	-0.35	0.41	F	NGC 4387	-0.01	0.02	P
NGC 1549	-0.20	0.16	F	NGC 4406	-0.15	0.03	P
NGC 1700	-0.25	0.08	F	NGC 4472	-0.15	0.04	P
NGC 2986	-0.15	0.13	F	NGC 4478	-0.12	0.06	P
NGC 7144	-0.32	0.17	F	NGC 4486	-0.23	0.05	P
NGC 7145	-0.31	0.22	F	NGC 4551	-0.01	0.03	P
NGC 7507	-0.04	0.17	F	NGC 4636	-0.22	0.05	P
NGC 7626	0.02	0.50	F	NGC 4649	-0.15	0.04	P
NGC 315	-0.08	0.10	P	NGC 4697	-0.18	0.04	P
NGC 720	-0.22	0.05	P	NGC 4874	-0.07	0.09	P
NGC 741	-0.26	0.17	P	NGC 4889	-0.08	0.06	P
NGC 1052	-0.17	0.03	P	NGC 5638	-0.19	0.05	P
NGC 1129	-0.02	0.09	P	NGC 5813	-0.05	0.04	P
NGC 1600	-0.19	0.06	P	NGC 5831	-0.10	0.04	P
Abell 496	-0.05	0.13	P	NGC 5845	0.01	0.03	P
NGC 2300	-0.20	0.13	P	IC 1101	-0.05	0.14	P
NGC 2768	-0.20	0.06	P	NGC 6051	0.10	0.09	P
NGC 2778	-0.13	0.04	P	NGC 6086	-0.15	0.08	P
NGC 2832	-0.13	0.06	P	NGC 6269	-0.04	0.14	P
NGC 3377	-0.24	0.03	P	NGC 7626	-0.18	0.08	P
NGC 3379	-0.19	0.01	P				

Mean $\Delta(U\text{-}B)/\Delta\log$ r from Peletier *et.al.* (1990) and Franx *et.al.* (1989)

(compare to Table 3.3 and Figure 3.3). Using their best-fit lines relating the escape velocity to *U-R* and *B-R*, we can estimate their measurements of Δ (*U-B*)/Δ log *r* to be 0.79 for the constant mass-to-light ratio model and 0.75 for the dark halo model. The merger remnants come rather close to Franx and Illingworth's models with a mean Δ (*U-B*)/Δ log *r* of 0.457. The mean falls

short by only 40%, indicating the mergers of spiral galaxies with color gradients can almost produce ellipticals with the proper gradients.

Conclusion

In the preceding section, the results of the merger hypothesis and a simple model of the color evolution during and after the merger (*i.e.* the stars do not change color) were compared with observations and measured up surprisingly well. However, in spite of these successes the inadequacies of the model outlined in the subsection "After the merger" still plague the analysis and may result in qualitative changes in the final color gradients of merger remnants. Regardless of these reservations, this first-order attempt to trace the evolution of color gradients indicates that mergers may be able to explain the color gradients in elliptical galaxies.

Bibliography

Barnes, J.E. and Hernquist, L. 1991, *Ap. J.*, **370**, L65.

Binney, James and Tremaine, Scott. 1987, *Galactic Dynamics*, (Princeton: Princeton University Press)

Boronson, Todd A., Thompson, Ian B. 1991, *A. J.*, **101**, 111.

Carlberg, R.G. 1984, *Ap. J.*, **286**, 403-415.

Couture, Jean, and Hardy, Eduardo. 1990, *A. J.*, **99**, 540.

Franx, Marijn, and Illingworth, Garth. 1990, *Ap. J. (Letters)*, **359**, L41-L45.

Franx, Marijn, Illingworth, Garth, and Heckman, Timothy. 1989, *A.J.*, **98**, 538.

Garnett D.R. and Shields G.A. 1987, *Ap. J.*, **317**, 82-101.

Larson, Richard B. 1974, *M.N.R.A.S.*, **166**, 585-616.

Peletier, Reynier F. *et. al.* 1990, *A.J.*, **100**, 1091.

Sandage, A.R., Becklin, E.E., Neugebauer, G. 1969, *Ap. J.*, **157**, 55.

Schweizer, François, Seitzer, Patrick, Faber, S.M., Burstein, David, Dalle Ore, Cristina M., Gonzalez, J. Jesus. 1990, *Ap. J. (Letters)*, **364**, L33-L36.

Walterbos, René. 1986, *Stars, Gas, and Dust in the Andromeda Galaxy.* PhD Thesis

Chapter 4: Velocity Mappings of Merger Remnants

Observations have only recently begun to explore the velocity distributions of elliptical galaxies. Measuring velocities in ellipticals has always been a more difficult task than in their spiral counterparts, and only with the recent improvements in observational techniques and technology have these observations become possible. With these new tools, observers showed that the rotational velocities of large elliptical galaxies were one-third what would be expected from their flattening (Bertola and Capaccioli 1975; Illingworth 1977), tearing asunder the notion that flattened elliptical galaxies were oblate rotators.

With each passing year, our knowledge of the velocity structure in ellipticals has increased substantially, greatly complicating our models of these galaxies. Franx, Illingworth and Heckman (1989) found that some ellipticals even rotate about their minor axes and others have counter-rotating regions. And even more strange, Rubin, Graham and Kenney (1992) found two cospatial stellar disks in the E7/S0 galaxy NGC 4550, one rotating prograde and one orbiting retrograde.

A question arises: can stellar dynamical mergers produce these strange features? But even more importantly, can they result in galaxies without such startling signatures, and are there more subtle features of merger remnants? From an examination of the present simulations, the answers to these three questions are all "yes". The variety of kinematic features possible seems to be

limited only by the variety of possible initial conditions. However, by making some theoretical considerations, the problem becomes a bit less intractable. The primary factor in the appearance of kinematic structure in the remnants is the amount angular momentum in the initial galaxies and how and to where it is transferred during the merger.

The Transfer of Angular Momentum

Without the possibility of transfer of angular momentum, mergers could never occur. Qualitatively, during the merger, the orbital angular momentum of the inner, more dense components is transferred outward to the less dense components and becomes spin angular momentum. The main mechanism for this transfer is dynamical friction which slows the motion the denser components relative to the less dense background. Binney and Tremaine (1987) lucidly explain dynamical friction and present some worked examples. Dynamical friction is essentially the process by which a point mass is decelerated while moving through a background distribution of particles with much smaller masses. The Chandrasekhar dynamical friction formula,

$$\frac{dv_M}{dt} = -16\pi^2 \ln\Lambda G^2 m(M+m) \frac{\int_0^{v_m} f(v_m) v_m^2 dv_m}{v_m^3} v_M, \qquad \textbf{(4.1)}$$

is the equation of motion of a point mass suffering this deceleration where Λ is the Coulomb logarithm and $f(v_m)$ is the distribution of velocities (v_m) of the background stars. For our analysis, the most important feature of this formula is that the force always points in the direction opposing the relative motion of the point mass and the background. Thus, in the "laboratory" frame, both the

background distribution of stars and the point mass suffer a change in velocity reducing their relative motion.

Hierarchial transfer

The discussion of dynamical friction above refers to the action of a smooth background density distribution upon a point mass, but mergers involve extended distributions of stars not point masses nor smooth density distributions. However, to a good approximation a more dense component may be considered equivalent to a point mass when it is travelling through a less dense region. Thus a hierarchy of momentum transfer naturally forms. The more dense components transfer their relative motion (orbital angular momentum) to the less dense components as spin angular momentum. From the disks to halos, the momentum flows, and then from the bulges to the disks.

Dark halos and angular momentum

The action of the dark halos on the orbital angular momentum is noticeable when examining the encounter from beginning to end. During the encounter NB00, both disks lose all their orbital angular momentum and some spin angular momentum. The only sink for this momentum are halo particles.

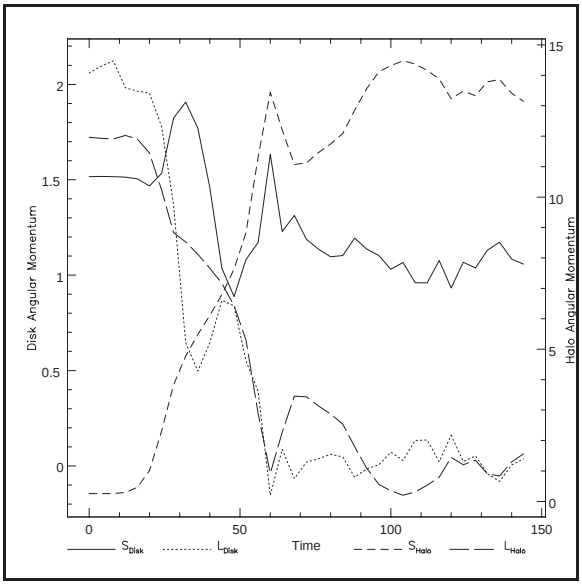

Figure 4.1 The evolution of L_z in Run NB00

However, even the massive halo doesn't have an unquenchable thirst for angular momentum as it must expand in order to absorb the angular momentum of the more compact components. The result is that the more compact components slowly sweep the halo particles out of the central region, reducing the halo's effectiveness at slowing the luminous parts of the galaxies through dynamical friction.

A prediction of this analysis is that the effective radius of the halo can be a determining factor in the evolution of the merger. For example if the halos are more diffuse that in these simulation, one would expect the merger to take longer or not to occur at all as the halos would be less efficient at absorbing the orbital angular momentum of the disks and bugles. On the other hand a more compact halo would quicken the merger once started, by thickening the amber in which the galaxies are trapped.

The point-mass approximation

Figure 4.2 depicts the distribution of angular momentum (in the z direction, measured relative to the center of mass of the entire system) and radius for all the luminous particles in the first galaxy of run NB00 at t = 16, 20, 24, and 28. What is startling about the plots is the correlation of the disturbance in the L_z versus r distribution with the position of the center of mass (marked with an X) of the second galaxy at that particular time. From t = 16 to t = 20, the particles near the center of mass of the second galaxy lose angular momentum in the z-direction. During this time, in the "laboratory

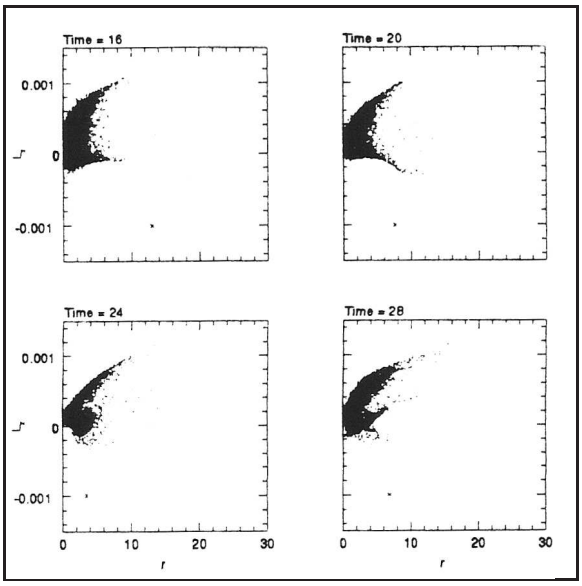

Figure 4.2 The Distribution of Particles in L_z and Radius from the Center of the Component; Galaxy #1, Run NB00

frame" the center of mass of the second galaxy is moving through the disk of the first galaxy in the same direction as the stars of the disk rotate. The second galaxy is moving more slowly than the stars in the first galaxy, resulting in a transfer of angular momentum from the stars to the second galaxy. This interpretation blatantly neglects the action of the halos which dominate the total angular momentum transfer. However, since the density gradient in the halo is less pronounced than that of the second galaxy, the influence of the halos varies less in time and in radius than that of the second galaxy's center of mass. Consequently, radial variations in transfer of angular momentum such as these are probably due to the influence of the second galaxy rather than the halos, but a further analysis of the torques between the components would be required to verify this assertion. In the following plots, the two galaxies reach pericenter and their maximum relative velocity. Here, the center of mass of the second galaxy is moving quickly enough for the transfer to go in the opposite direction, and a tilted U-shaped distribution results.

Furthermore, when one examines the analogous distributions for the

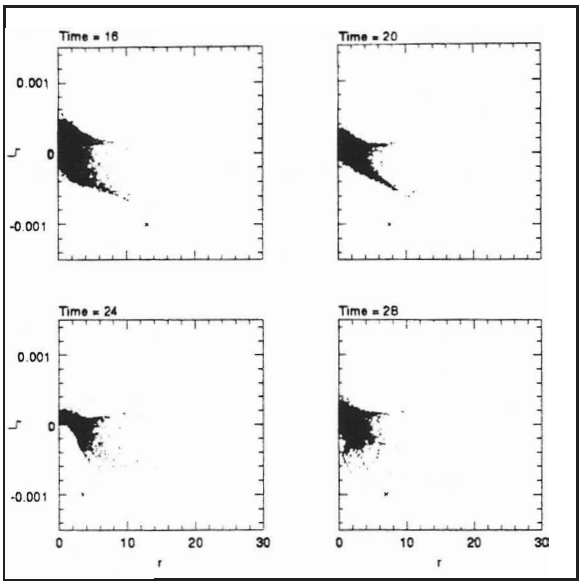

Figure 4.3 The Distribution of Particles in L_z and Radius from the Center of the Component; Galaxy #2, Run NB02

first galaxy in simulation NB02, the picture is nearly identical. On the other hand, the picture for the second galaxy in NB02 or equivalently for either galaxy in NB22 is quite different. Figure 4.3 depicts the distribution for the former case. Here the transfer of momentum between the disk of the second galaxy to the center of mass of the first is again noticeable, but the picture is much more difficult to interpret.

An important corollary of this point-mass approximation is that the fate of the distribution of angular momentum in one galaxy is not affected strongly by the distribution of angular momentum in the other galaxy. Thus, one would expect the final distribution of angular momentum for the particles initially belonging to one galaxy only to depend on the initial distribution of $\boldsymbol{L}$ and mass throughout that galaxy and on the orbital parameters.

Runs NB00, NB02, and NB22 give us the opportunity to put this supposition to the test. In the remnants of these runs, the final distribution of particles originally in the prograde component of NB02 is nearly identical to the distribution of particles in either component of NB00. Furthermore, the

distribution of those particles originally in the retrograde component of NB02 is nearly identical to those in NB22. Also, the time evolution of the total spin and orbital momentum are quite similar for these pairs of components. In essence the mapping from the initial to final distribution for one component is independent of the details of the second component's distribution, or in mathematical notation, where *M* is the mapping for the entire system and *m* is a mapping for one component, and *A* and *B* are the initial distributions for each component, we have

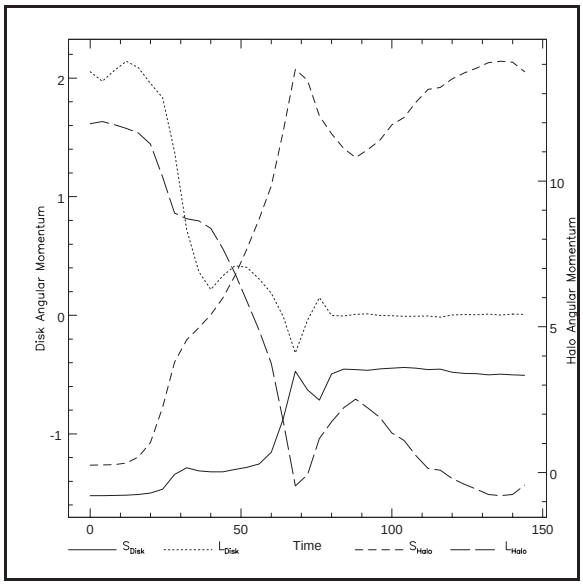

Figure 4.4 The evolution of L_z in Run NB22

$$M_{i\to f}(A+B) = m_{i\to f}(A) + m_{i\to f}(B). \qquad \textbf{(4.2)}$$

With this knowledge, one could have predicted the final distribution of L_z and *r* for NB02 by taking a single component from the remnant NB00 and one from NB22 and superposing their distributions. Although this is an interesting result, it is far from exact as it blatantly disregards the parameters that were not varied in three simulations examined, such as the presence of a bulge (or more general variations in the radial mass distribution) and misalignment of a disk with the orbital plane. However, it does provide a rule of thumb for predicting the appearance of remnants from the initial conditions before performing a simulation.

Misalignment of Kinematic Axes

The remnants especially those from the less symmetric runs showed a great variety of kinematic properties; some of the more obvious were misalignments between the rotation axis and the major axis of the remnant and the rotation axes for shells of matter at different radii from the center. The major axis for a given shell was taken to point in the direction of the eigenvector of the inertia tensor (of the matter in the given shell) that had the largest eigenvalue. For an axisymmetric oblate rotator, one would expect the axis of rotation to always point along this eigenvector. In more general, triaxial distributions supported by velocity anisotropy, there need not be a correlation between the apparent rotation axis and the major axis of the distribution.

For the remnants, as outline above, the rotation axis and the major axis were calculated for the three-dimensional mass distribution of the remnant. No attempt was made to project these distributions and to measure the rotation and major axes as an observer would. Rather, we assume that one could observe the projection of these "three-dimensional" axes into the image plane, and the angle that one would measure between them would be

$$\sin\theta_{observed} = \sin\theta_{3-D}\cos\phi \qquad \textbf{(4.3)}$$

where ϕ is the angle between the image plane and the plane containing the two vectors. Thus, if one knows the distribution of $\theta_{3\text{-}D}$, one can calculate the distribution of $\theta_{observed}$.

The current set of runs does not explore the initial parameter space

Table 4.1 Misalignment Angles between Photometric and Kinetic Axes

Run Code	Radius 0 - 1	Radius 1 - 2	Radius 2 - 3	Radius 3 - 4	Radius 4 - 5
NB00	6.1	10.2	10.9	13.4	9.6
OB00	3.3	9.1	4.0	9.3	7.3
RB00	9.2	11.5	9.9	11.0	5.7
NB02	61.2	42.2	10.2	22.5	20.1
OB02	73.6	12.5	9.7	7.1	9.7
RB02	78.3	52.1	17.1	26.0	32.5
NB01	81.3	68.7	49.9	59.1	71.8
OB01	63.4	28.5	60.1	58.0	70.0
RB01	39.9	54.0	62.4	67.1	73.1
NB11	65.1	82.1	76.8	76.8	79.1
OB11	64.8	88.3	86.2	87.2	82.4
RB11	62.9	87.3	81.8	86.7	81.8
NB22	62.8	7.0	1.0	11.5	8.4

realistically enough to perform this exercise. Rather the simulations provide a qualitative look at the misalignments possible in merger remnants. The misalignments between the photometric and kinetic axes as expected are largest in the collisions without the disks aligned with the orbital plane. As discussed in Chapter 2, the initial conditions of the interaction designate one or more preferred planes which coincide with the planes of the orbit and the disks. However, except in regions of the remnant where the initial spin angular momentum dominates the final distribution of momenta, as far as kinematic properties are concerned the orbital plane is dominant. From the

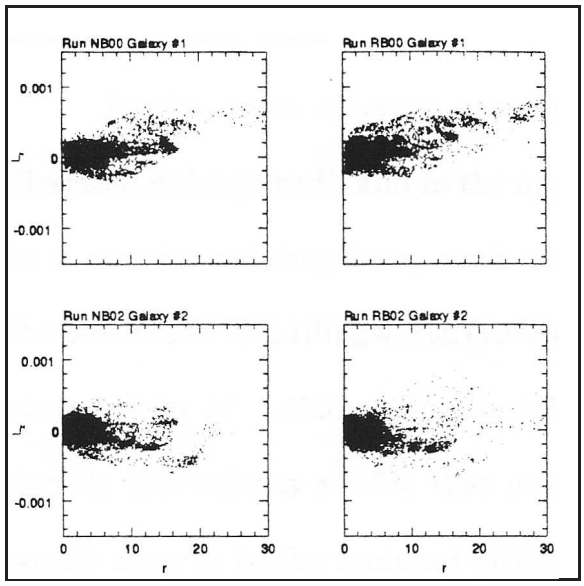

Figure 4.5 Final Distribution of L_z for Galaxy #1 in NB00 and RB00, and Galaxy #2 in NB02 and RB02

process of hierarchial transfer in which the outer, less dense components absorb the orbital angular momentum of the inner components, one would expect the initial spins to define the preferred kinetic axis at small radii while the initial orbital angular momentum to determine it at larger radii.

To illustrate this effect, Figure 4.5 compares the final distribution of L_z versus radius for the runs NB00, RB00, NB02, and RB02 for components with their spin initially aligned with the orbital angular momentum and those with their spins initially antialigned. Furthermore, the cases with rotating bulges are included to depict the effect of increasing the initial spin at small radii. In these most extreme cases, one can see the shift of dominance from spin to orbital angular momentum as one shifts one's attention from small to large radii. In the cases with disks not aligned with the orbital plane, this effect causes the preferred kinetic plane to shift from the initial disk planes to the orbital plane with increasing radius.

Counterrotating cores

In the most extreme case, the angular velocity may point in one

direction at large radii and in the opposite direction near the center, resulting in a counter-rotating core, such as the one Franx and Illingworth (1988) observed in IC 1459. Figure 4.6 depicts the velocity profile that one would observe in the remnant OB02 from a viewpoint near the initial orbital plane. At small radii (less than about 20 kpc), the remnant is rotating in the opposite sense at the initial orbital angular momentum, while at larger radii it rotates in the same direction. The counterrotation in the remnant is neither as strong as in IC 1459 (peak velocity of 50 km/s versus 200 km/s) nor as confined in a compact core (the counterrotating regions have radii of 20 kpc versus 3 kpc). However, the effect qualitatively is the same.

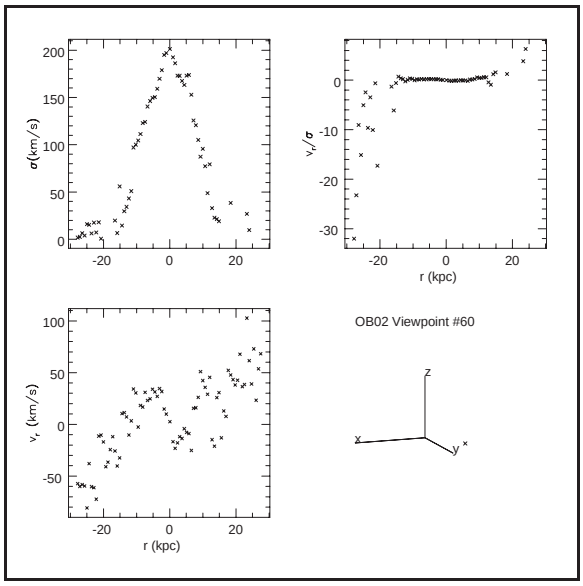

Figure 4.6 Velocity Profile for Run OB02

The remnant NB22, whose velocity profile as observed from near the initial orbital plane, is depicted in Figure 4.7. In this remnant the counterrotating region is much larger consisting of nearly the entirely galaxy. However at very large radii (greater than 50 kpc), the particles orbit in the same sense as the initial orbit, and one would expect to observe a large shell rotating counter to the rest of the galaxy.

Velocity Dispersion and Rotation

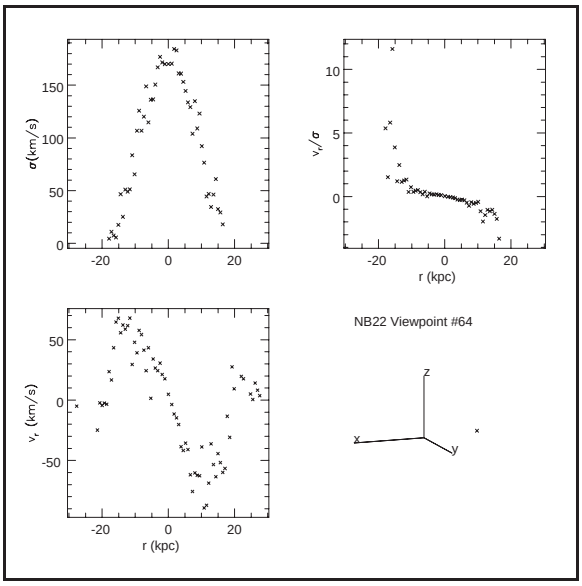

Figure 4.7 Velocity Profile for Run NB22

The velocity fields of the merger remnants also show more subtle features than misalignments. The most general signature is an increase in v_r with radius accompanied by a decrease in σ, thus v_r/σ may vary from a few tenths near the center of the remnant for a few toward the edges. Figure 4.8 presents the velocity profile of remnant NB00 as viewed from near the initial orbital plane. From this viewpoint, if one ignores the velocity dispersion, the remnant appears to have the rotational velocity profile of a rigid rotator over a large range in radii. This feature also results from hierarchial transfer as more orbital angular momentum and therefore rotational velocity is deposited at large radii than at small.

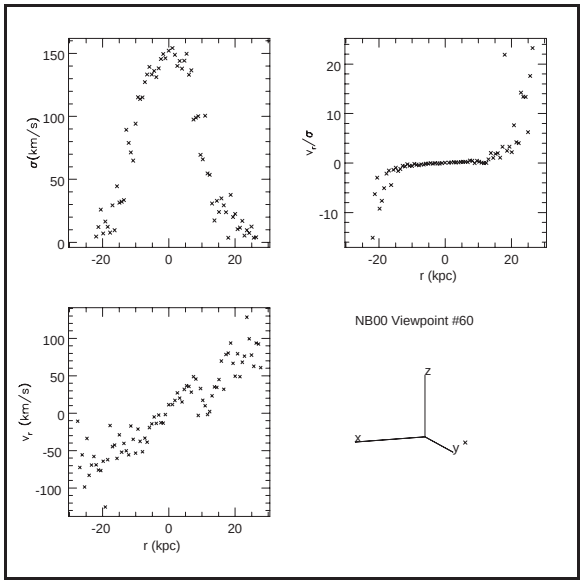

Figure 4.8 Velocity Profile for Run NB00

In Franx, Illingworth, and Heckman's (1989) sample of 22 elliptical galaxies, two (NGC 1395, NGC 1407) show this effect strongly while another

five may show this feature more weakly. None of the galaxies their sample show the sharp dropoff in velocity dispersion found in NB00; unfortunately, the sharp decline from 150 km/s to on order of 20 km/s did occurred at a radius of about 20 kpc which was outside the purview of Franx, Illingworth and Heckman's observations. However, the line of sight dispersion did decline with radius at least slightly in all the galaxies in the sample.

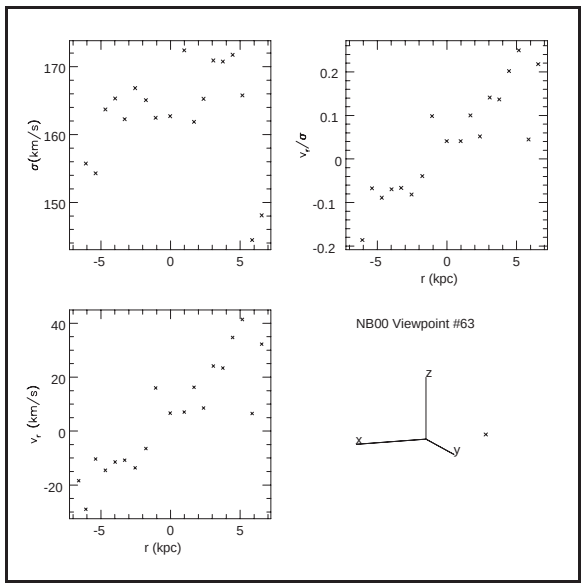

Figure 4.9 Central V $_r$ Profile for Run NB00

Figure 4.9 depicts the velocity profile at a slightly different viewpoint for the same run, NB00 and focuses on the inner 5 kpc. Again the linear increase of v_r is noticeable as well as an increase of v_r/σ with radius. In this region the value of σ does not decrease markedly as over the larger scale. This linear increase of v_r with radius appears to be a general feature of the more symmetric mergers when viewed from near the original orbital plane.

A Preliminary Model of NGC 4550

Rubin, Graham and Kenney (1992) discovered that the E7/S0 galaxy NGC 4550 has two cospatial stellar disks, one rotating prograde and one retrograde. Figure 4.10 depicts the velocity field in the orbital plane of remnant NB02 as viewed from near the axis of the initial orbit. The figure

does not display the flow in the usual manner. To interpret the figure, one must consider that two wind vanes are attached to each cross. One vane only feels the "wind" of the flow of stars originally in the galaxy initial rotating prograde and the second vane, only the "wind" from the galaxy initially rotating retrograde.

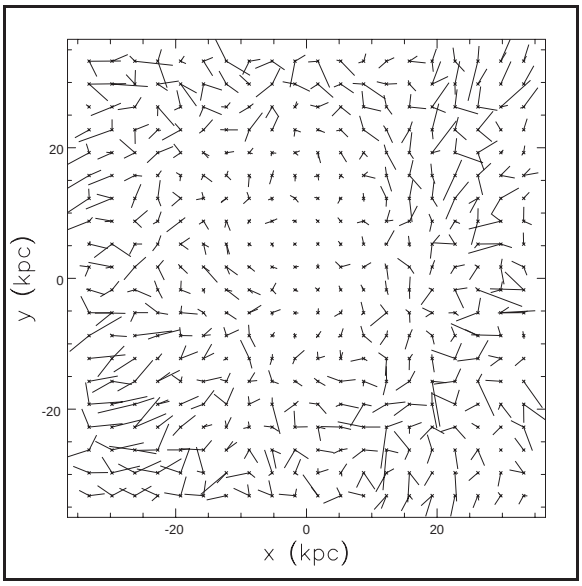

Figure 4.10 Velocity Field for Run NB02

The interesting result is that at many of the grid points the stars initially in one galaxy flow in one direction and those initially in the other flow in the other direction. One could have predicted this result from the "superposition" principle explored in a previous section. Rubin, Graham, and Kenney may be observing a galaxy similar to this simulated remnant from a viewpoint in the initial orbital plane of the merging galaxies (edge-on). They suggest that the counterrotating population of stars form from the counterrotating gas after the gas had settled into the plane of the galaxy. However, a purely stellar dynamical merger similar to NB02 could produce a similar distribution.

From this model NGC 4550, one would expect the galaxy to have a lower central phase space density than an elliptical galaxy with the same luminosity. From the analysis in Chapter 5 and this model, we predict that the central phase-space density is at least 6×10^{-9} $M_{\odot}$ pc^{-3} $(km/s)^{-3}$ and no more than about

6×10^{-8} $M_{\odot}$ pc^{-3} $(km/s)^{-3}$, much less than ellipticals with comparable luminosities. Further analysis of the simulated remnant and comparison with the observations is necessary to determine the plausibility of this conjecture.

Conclusion

Mergers can produce much of the variety found in the kinetics of elliptical galaxies, such as counterrotating cores, shells, and kinetic misalignment. However, mergers can leave some more subtle features that are not found many ellipticals such as the increase of rotational velocity with radius, but these signatures may not be observable from all viewpoints. Exploration of merger remnants both over a realistic distribution of initial conditions and over viewing angle would necessary to determine the frequency of these features.

Bibliography

Bertola, F. and Capaccioli, M. 1975, *Ap. J.*, **200**, 439.

Binney, J.J., Davies, Roger L., and Illingworth, Garth D. 1990, *Ap. J.*, **361**, 78-97.

Binney, James and Tremaine, Scott. 1987, *Galactic Dynamics*, (Princeton: Princeton University Press)

Franx, M, and Illingworth, G.D. 1988, *Ap. J. (Letters)*, **327**, L55.

Franx, Marijn, Illingworth, Garth, and Heckman, Timothy. 1989, *Ap. J.*, **344**, 613-636.

Illingworth, G. 1977, *Ap. J. (Letters)*, **218**, L43.

Rubin, Vera C., Graham, J.A., and Kenney, Jeffrey D.P. 1992, "Cospatial Counterrotating Stellar Disks in the Virgo E7/S0 Galaxy NGC 4550"

Chapter 5: The Phase-Space Density Problem

Probably the most persistent problem for the merger hypothesis is revealed when the central phase-space densities for elliptical galaxies is compared with the central phase-space densities of spiral galaxies (Carlberg 1986). The central phase-space densities (f_c) of spirals falls short of the value of ellipticals with similar luminosities by a factor of 100 or more. Furthermore, as will be explained in the following section, unfortunately during a purely stellar dynamical merger, the maximum microscopic phase-space density must remain constant, while the macroscopic (*i.e.* measurable) maximum f can only decrease.

Many solutions have been proposed for this problem. Lake (1989) proposed the material with high phase-space densities from the outer regions of spiral disks could fall inward and carry its high f to the center. However, it is rather difficult to propose a stellar dynamical method to achieve this. In Chapter 3, it was shown that during the merger, generally, particles keep their radial order, and very few, if any at all travel from the outer edges to the center. Furthermore, from the process of hierarchial transfer of angular momentum outlined in the chapter exploring velocity mappings, one would expect the outermost particles to absorb angular momentum from the inner regions and to move to larger (not smaller) radii.

This chapter will explore a second solution. The set of merger simulations has neglected an important component of spiral galaxies, the gas.

We will examine whether an extreme model of gas dynamics during the merger can produce the observed central phase-space densities in ellipticals.

Why is There a Problem?

The problem stated bluntly is that phase fluid is incompressible. During stellar dynamical mergers, the phase-space density evolves according to the coupled Boltzmann and Poisson equations:

$$\frac{\partial f_k}{\partial t} + \boldsymbol{v}\cdot\frac{\partial f_k}{\partial \boldsymbol{x}} - \nabla\phi\cdot\frac{\partial f_k}{\partial \boldsymbol{v}} = 0$$
$$\nabla^2\phi = 4\pi G\int d\boldsymbol{v}\,(f_1 + f_2). \qquad \textbf{(5.1)}$$

These equations simplify significantly if one moves into Lagrange coordinates which move through phase space with a given bit of phase fluid to

$$\frac{df}{dt} = 0. \qquad \textbf{(5.2)}$$

This is essentially a restatement of Liouville's theorem. Let's follow the patch of maximum phase-space density in the progenitor spiral galaxies. Although during the merger it may move through phase space, the value of *f* within the patch will remain constant, and it will still be the maximum *f* in the remnant. Furthermore, as discussed in Chapter 3, patches of phase space do not move drastically in radius during the merger, therefore the maximum phase density near the centers of the progenitor spirals will map to the maximum phase density near the center of the remnant. Furthermore, the coarse-grained or observable phase-space density can decrease as empty phase space ("air") is mixed in with populated regions of phase space. Unfortunately for the merger hypothesis, the central densities in spirals fall short of those in ellipticals with

similar luminosities by a factor of a hundred or so, and the collisionless Boltzmann equation cannot provide an avenue for their increase.

Phase Densities in the Simulated Remnants

The evolution of the phase space density in the current set of simulated mergers follows the collisionless Boltzmann equation and therefore will decrease or remain the same but not to increase. After the merger Hubble profiles were fit to the three-dimensional distribution of luminous matter in remnants to find the core radius of each remnant. Following the method of Carlberg (1986), the central phase-space density was estimated to be

Table 5.1 Central Phase-Space Densities of the Simulated Remnants

Run Code	σ_c (km/s)	r_c (kpc)	f_c 10^{-8} $M_\odot$ pc^{-3} $(km/s)^{-3}$
NB00	287	1.29	2.21
OB00	320	0.64	8.04
RB00	324	0.93	3.79
NB02	293	2.56	0.55
OB02	316	2.39	0.58
RB02	321	2.32	0.61
NB01	259	2.62	0.59
OB01	271	2.64	0.56
RB01	276	1.19	2.70
NB11	277	1.00	3.80
OB11	308	1.46	1.60
RB11	304	1.00	3.47
NB22	292	1.46	1.70

$$f_c = 10.5\,\mathrm{M_\odot pc^{-3}(km\,s^{-1})^{-3}}\left(\frac{\sigma_c}{1\,\mathrm{km/s}}\right)^{-1}\left(\frac{r_c}{1\,\mathrm{pc}}\right)^{-2}. \qquad \textbf{(5.3)}$$

The central value of σ was estimated by taking the trace of the velocity tensor in an radial shell 350 pc thick containing r_c. Table 5.1 lists the final phase-

space densities for the thirteen remnants.

These final phase-space densities agree with the predictions of the collisionless Boltzmann equation, and Carlberg's (1986) estimate of the central phase-space density of the Milky Way ($\approx 2.5 \times 10^{-8}$ $M_\odot$ pc^{-3} $(km/s)^{-3}$). Carlberg also estimates the central phase-space density of an elliptical galaxy with twice the luminosity of the Milky Way to be approximately 4×10^{-6} $M_\odot$ pc^{-3} $(km/s)^{-3}$. The results of the mergers fall short by a factor of 50 to 700.

Gas Dynamics

The presence of gas in spiral galaxies is often cited as a way out of this problem. Unlike stars, the gas is compressible, can cool, and its density could reach arbitrarily high values if the gas is compressed arbitrarily close to the center of the remnant. According to Barnes and Hernquist (1992), after the merger, the remnants are often left with a massive nuclear concentration of gas. Furthermore, the observations imply that the compression due to shocks will spark a wave of star formation involving most of this central gas.

A Very Much Simplified Gas Dynamical Model

To try solve this problem, we will take an extreme gas dynamical model in which all the gas initially in the galaxy flows to the center of the remnant after the merger. Then by comparing the new half-mass radii with the old half-mass radii, we can estimate the increase in the observed central phase-space density due to this process. From Eqs. (5.2), (5.3), and assuming that the core radius and velocity dispersion scale as the half-mass radius and the

velocity dispersion at the half-mass radius, we get

$$\frac{f_f}{f_i} = \left(\frac{r_i}{r_f}\right)^2 \frac{\sigma_i}{\sigma_f}. \qquad \textbf{(5.4)}$$

The observable velocity dispersion may also scale with the change in radius, as a result of the virial theorem,

$$\left(\frac{\sigma_f}{\sigma_i}\right)^2 = \frac{\dfrac{G(0.5M_T)}{r_{\frac{1}{2},f}}}{\dfrac{G(0.5M_T)}{r_{\frac{1}{2},i}}} = \frac{r_{\frac{1}{2},i}}{r_{\frac{1}{2},f}}, \qquad \textbf{(5.5)}$$

Thus to determine the phase-space density we must determine the change in half-mass radius due to the gas.

As the entire mass of gas (μ) flows to the center, the half-mass radius shrinks until it is equal to a radius, r_{ε}. This radius initially contains a mass fraction ε which is the difference of one-half and the amount of gas that flows from outside r_{ε} to the center, so now half the luminous mass of the galaxy resides within r_{ε}. There are two cases, one where all the gas is initially outside r_{ε} and one where the gas to total mass ratio is constant with respect to radius. After the gas has moved to the center, we would like r_{ε} to contain half the total mass, therefore we get for the two cases

$$\epsilon + \mu = \frac{1}{2} \text{ and } \epsilon + (1-\epsilon)\mu = \frac{1}{2}. \qquad \textbf{(5.6)}$$

and solving for ε in these two cases gives

$$\epsilon = \frac{1}{2} - \mu \text{ and } \epsilon = \frac{\frac{1}{2} - \mu}{1 - \mu}. \qquad \textbf{(5.7)}$$

We assume that the gas flows adiabatically to the center, therefore the region

containing half the mass will shrink, as the product of the mass within r and r may be taken as an invariant (Blumenthal *et. al.* 1986). Since the initial mass fraction within r_ε is ε and in the end is one-half, after shrinking

$$r_{\frac{1}{2},f} = 2\epsilon r_{\epsilon}. \tag{5.8}$$

Next, to calculate the ratio of $r_{1/2,f}$ to $r_{1/2,i}$, we must assume a density model and determine the ratio of r_ε to $r_{1/2,i}$. We use the Hernquist model for elliptical galaxies,

$$\rho(r) = \frac{M_T r_0}{2\pi} \frac{1}{r(r+r_0)^3}, \tag{5.9}$$

where M_T is the total luminous mass of the galaxy. This model has quite nice analytic properties and fits the observations of elliptical galaxies and simulated merger remnants well (Hernquist 1992). Integrating Eq. (5.9) to find the mass within a given radius yields

$$M_r = M_T \frac{r^2}{(r_o + r)^2}. \tag{5.10}$$

Here M_r equals ε M_T, and inverting Eq. (5.10) yields

$$r_\epsilon = \frac{\sqrt{\epsilon}}{1-\sqrt{\epsilon}} r_0. \tag{5.11}$$

We may substitute one-half for ε to find $r_{1/2,i}$ in terms of r_0, then by combining this result with Eq. (5.8), we obtain

$$\frac{r_{\frac{1}{2},f}}{r_{\frac{1}{2},i}} = 2\epsilon \left(\frac{\sqrt{\epsilon}+\epsilon}{1-\epsilon} \right) \left(\frac{1}{\sqrt{2}+1} \right). \tag{5.12}$$

When Eq. (5.12) is combined with Eqs. ? and (5.7), the increase in phase-space density for a given gas fraction, μ, and set of assumptions may be calculated. Furthermore, Eq. (5.12) may be inverted to yield

$$\epsilon = -k\frac{1+\sqrt{2}}{3} + k^2\frac{3+2\sqrt{2}}{6D} + \frac{D}{6} \tag{5.13}$$

where

$$D = \sqrt[3]{(81+54\sqrt{2})k^2 + (7+5\sqrt{2})k^3 + 3\sqrt{3}k^2\sqrt{459+324\sqrt{2}+(82+58\sqrt{2})k}} \tag{5.14}$$

and

$$k = \frac{r_f}{r_i}$$

which gives the gas fraction necessary to produce a given increase in phase-space density.

How much gas?

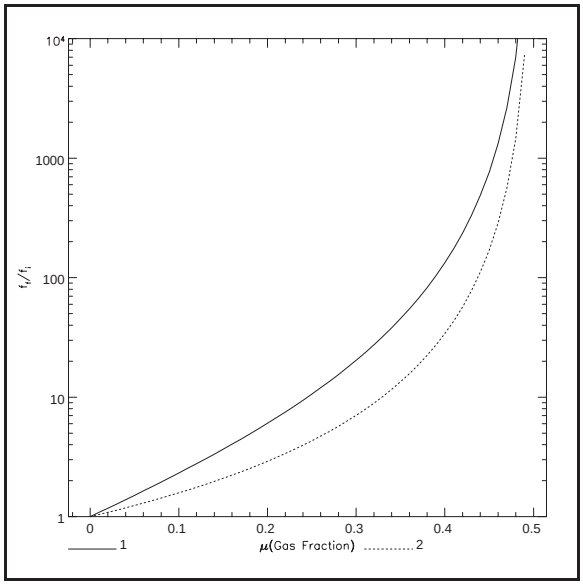

Figure 5.1 depicts the increase in observed phase-space density due to the flow of gas to the center of the merger remnant. Each of the four cases are depicted for a range of initial gas fractions from 0 to 0.5. According to our assumption that all the gas flows to the center, the ratio of final to initial phase-space density must diverge for gas fractions greater than one-half, because in this case the new half-mass radius will be zero. The four cases are as follows:

1. All the gas is initially outside r_{ε}.
2. The ratio of gas to total mass is initially constant with respect to radius.

The case 1 gives the largest increase in central phase-space density for a given gas fraction, and therefore in a way represents the best that the merger hypothesis can do. To increase in the central phase-space density fifty-fold which would bring the best case simulation (OB00) in line with the observations of ellipticals would require a gas fraction in the progenitors of 36% which is substantially more than is found in present-day spiral galaxies.

Conclusion

The model explored above represents the best-case scenario for the formation of elliptical galaxies through mergers. From the amount of gas needed to give the central phase-space densities of ellipticals in the center of remnants, one may conclude that ordinary ellipticals did not form through the mergers of present-day spirals. However, this calculation does not preclude the formation of high luminosity ellipticals through the multiple mergers of spirals nor the formation of ordinary ellipticals through the mergers of gassy spirals of earlier epochs. With the second option, the merger hypothesis converges with the dissipational theories of the formation of elliptical galaxies.

The analysis leads to another problem. Toomre (1977) and Vorontsov-Vel'yaminov (1977) predicted that most galaxies have been involved in encounters of one sort or another. If mergers are as common as these authors predict, where are all "very old tumbled remains that one should see today"? They cannot easily mask as normal elliptical galaxies; consequently, there must be a large population of puffy ellipticals with low central phase-space

densities, or Toomre and Vorontsov-Vel'yaminov have overestimated the frequency of mergers.

Bibliography

Barnes, Joshua E., and Hernquist, Lars, 1992, "Dynamics of Interacting Galaxies", Preprint

Blumenthal, George R., Faber, S.M., Flores, Ricardo, and Primack, Joel R. 1986, *Ap. J.*, **301**, 27.

Carlberg, R.G. 1986, *Ap. J.*, **310**, 593-596.

Carlberg, R.G. Lake, George, Norman, C.A. 1986, *Ap. J. (Letters)*, **300**, L1-4.

Hernquist, Lars. 1992, "Structure of Merger Remnants I. Bulgeless Progenitors" Preprint.

Lake, George. 1989, *A. J.*, **97**, 5.

Lake, George, Dressler, Alan. 1986, *Ap. J.*, **310**, 605-612.

Toomre, A. 1977, in *The Evolution of Galaxies and Stellar Populations*. ed. B.M. Tinsley and R.B. Larson (New Haven: Yale University Observatory), 401.

Vorontsov-Vel'yaminov, B.A. 1977, *Pis'ma v Astronomicheskij Zhurnal*, **3**, 251.

Chapter 6: Concluding Remarks

After examining the remnants of the thirteen simulated mergers, one can see that mergers produce galaxies that qualitatively resemble elliptical galaxies in their mass distribution, photometry and kinetics. For many features, the resemblance is quantitative as well; however, in one important respect the characteristics of these remnants deviate from those of ordinary ellipticals. Chapter 5 examined the observable phase-space densities of merger remnants and the effect of gas dynamics on these quantities. The remnants unless the progenitors contain a large amount of gas, fall short of elliptical galaxies with similar luminosities by a large factor. However, the calculations of Toomre (1977) and Vorontsov-Vel'yaminov (1977) indicate that mergers probably have played an important role in galaxy evolution.

Getting Mergers to Work

The previous chapters cited the presence of gas in the progenitor galaxies as a possible panacea for the discrepancies between merger remnants and elliptical galaxies. Chapter 3 discussed the importance of star formation sparked by the merger and its effects on the final color gradients of the remnant. Chapter 5 examined how gas dynamics affects the final phase-space densities of the remnants. Although the chapter concluded that spiral galaxies of today with an ordinary fraction of their mass in gas could not merge into normal ellipticals, two possibilities exist. The merger of spirals that have an extraordinary amounts of gas for today, or the merger of yesterday's spirals

could produce "normal" ellipticals, Or, the merger of ordinary spirals could result in anomalous, "puffy" ellipticals.

A few studies have tried to tackle the difficult task of including realistic gas dynamics in their simulations (Umemura and Yoshioka 1990; Barnes and Hernquist 1991; Noguchi 1991). All three of these simulations found that qualitatively the gas tends to collect at the center of the merger remnant. Barnes and Hernquist, and Noguchi posit this central gas cloud may fuel violent star formation and star bursts. However, further steps must be taken to study gas processes. All three of these studies omit a different aspect of the interaction. Umemura and Yoshioka's progenitor galaxies lack dark halos which in many respects chart the course of the interaction (Chapter 4). Barnes and Hernquist collide galaxies with initially smooth gas distributions, neglecting the clumpiness of the molecular gas in spiral galaxies. Although Noguchi unlike the other researchers considers the effects of star formation and supernovae on the final gas distribution and models the gas as "sticky" clouds, his calculations neglect the gravity of the gas and therefore are not fully self-consistent.

A merger simulation including realistic gas dynamics with some model of star formation and supernovae is an important and necessary next step toward a fuller understanding of galaxy interactions and evolution.

The Importance of Mergers in Galaxy Evolution

The discrepancy between the estimates of the merger rate over the

history of the universe (Toomre 1977; Vorontzov-Vel'yaminov 1977) and the number of potential merger remnants seen today opens up a question of the validity of these estimates. Carlberg (1990) proposes using mergers as an estimate of Ω. He calculates that merger rate varies as $(1+z)^{m}$ where $m \simeq 4.51\Omega^{0.42}$. By integrating the number of mergers that occurred over the age of the universe using this rate and comparing this value with the number of merger remnants, Ω could be determined in a rather straight-forward manner. However, what constitutes a merger remnant strongly depends on the structure of the progenitor galaxies, especially the gas fraction. Therefore, a complete analysis of this problem would require simulating the mergers of the gas-rich progenitor galaxies presumed to inhabit the early universe as well as contemporary galaxies and comparing the remnants with galaxies observed today. In spite of these difficulties, the method may provide a unique method to determine the fate of the universe.

Further Research

Further initiatives in this field may naturally be divided into three paths.

Analysis

First is the further analysis of existing simulations. The analysis of each of the preceding chapters may be improved. The analysis of the isophotes must be performed in a manner more in agreement with the methods used by observers. Rather the fitting a path to the images by minimizing a least-

squares sum, the observations used for comparison in Chapter 2 generally use some type of Fourier decomposition to iterate the path. This difference weakens the conclusions of the chapter and must be rectified for future investigations.

The analysis of the other chapters may improved by fitting projected mass distributions rather than the three-dimensional distribution to bring this analysis in coincidence with the observations. Also in the spirit of reconciling the analysis with observational techniques would be to determine the location of the merger remnants with respect to the fundamental plane of elliptical galaxies (Dressler *et. al.* 1987) and the effect of gas dynamics on their positions. Furthermore, an examination of metallicity gradients instead of color gradients could more reliably probe the final appearance of merger remnants in both color and metallicity. And finally a thorough look at the actual torques between the various components during the merger would elucidate the transfer of angular momentum and the creation of the velocity fields in the remnants.

Simulations

As a previous section hints, a merger simulation including realistic gas dynamics with some model of star formation and supernovae heads the wish list. Also in the vein of more realistic simulations would be the inclusion of chemical and stellar evolution; however, this goal is probably a long way off. In the short term, simulations with higher particle number would allow a more

thorough study of the photometry of the remnants, both in terms of isophote analysis and estimates of the central phase-space densities. Finally, to determine definitively what a typical merger remnant looks like a broader coverage of the space of initial conditions will be necessary.

To achieve these goals a two-pronged approach would probably be most useful. To examine the variety of initial conditions, smaller numbers of collisionless particles could quickly yield new results. Also, a small-scale simulation would be appropriate to get a better look at the role of gas dynamics and star formation. This would leave the largest and most time-consuming simulations to explore the photometry of the remnants where the largest strides could be made.

Observations

In the realm of observations, we can follow two paths. First is to observe present-day galaxies in the process of merging to gain a further understanding of the important physics in galaxy interactions and to estimate the current merger rate. Second is to more thoroughly observe the properties of suspected merger remnants - elliptical galaxies. An important comparison would be to measure the photometry of field versus cluster ellipticals, a task in the spirit of the investigation of Carvalho and Djorgovski (1992). The goal would be to measure the peak phase-space density in these objects to determine if cluster ellipticals have an earlier, if not entirely different formation mechanism than field ellipticals. A tempting speculation is that

field ellipticals formed from the recent mergers of the small, tightly bound clusters (Hickson 1982). Continuing with this speculation, one would expect that field ellipticals would have lower peak phase-space densities than their cousins in clusters.

Conclusion

The investigation of this thesis has essentially shown that the ordinary spiral galaxies of today cannot merge to form today's ordinary elliptical galaxies. However, it does not close the door on the merger hypothesis. Rather, it has opened many new questions for both observers and theoreticians as to the formation mechanism for elliptical galaxies over the history of the universe and hopefully has elucidated how merger remnants would appear to today's observers.

Bibliography

Barnes, J.E. and Hernquist, L. 1991, *Ap. J.*, **370**, L65.

Carlberg, R.G. 1990, *Ap. J.*, **359**, L1.

Carvalho, R.R. and Djorgovski, S. 1992, *Ap. J.*, **389**, L49.

Dressler, Alan, *et. al.* 1987, *Ap. J.*, **313**, 42.

Hickson, P. 1982, *Ap. J.*, **255**, 382.

Noguchi, M. 1991, *M.N.R.A.S.*, **251**, 360.

Toomre, A. 1977, in *The Evolution of Galaxies and Stellar Populations*. ed. B.M. Tinsley and R.B. Larson (New Haven: Yale University Observatory), 401.

Umemura, M. and Yoshioka S., 1991, in *Primordial Nucleosynthesis and Evolution of Early Universe*. ed. K. Sato and J. Audouze, 565.

Vorontzov-Vel'yaminov, B.A. 1977, *Pis'ma v Astronomicheskij Zhurnal*, **3**, 251-253.

Appendix A: Russian Sources in the Area

Like the research performed elsewhere, Soviet and now Russian advances in the study of galaxy interactions have taken three paths. First are observations of peculiar and interacting galaxies with the extensive catalogs of Vorontsov-Vel'yaminov (1959) and Arp (1966) as the prime examples. Second are analytic theoretical investigations examining the formation of elliptical galaxies (Pol'yachenko 1991). Third is the method of this thesis, numerical simulation, which follows in the tradition of the works of Tashpulatov (1969, 1970), and Toomre and Toomre (1972). Not surprising, Soviet researchers over the past decades have divided their attention between these avenues in a unique manner. In recent years, the lack of access to computers, with speeds comparable to those available elsewhere, often became a deciding factor against performing numerical simulations. Consequently, since Tashpulatov's work, the Soviet studies on galaxy interactions have focused on the first two avenues: observation and analytic theory.

Initial Works

In late sixties, Tashpulatov's (1969; 1970) work on interacting galaxies set a precedent for the use of computers in the study of interacting galaxies. The simulations that have come since have been more extensive and more complicated, but the basic premise of simulating of these phenomena numerically came in part from Tashpulatov. The objective of his study was to determine whether tidal tails and bridges could form during the encounter of

two galaxies. He modeled the perturbed galaxy as a prolate ellipsoid and the perturbing galaxy as a point mass on a parabolic trajectory relative to the center of mass of the system.

During the interaction he assumed that the gravitational field of the elliptical galaxy was constant, or in other words, that the passage of the point-like galaxy did not affect the distribution of matter in the elliptical galaxy. The simulation calculated numerically the trajectories of test particles released from the vertex of the elliptical galaxy at equally spaced intervals of time during the encounter, and then Tashpulatov looked at the distribution of these test particles at later times to see whether features resembling tails or bridges had formed.

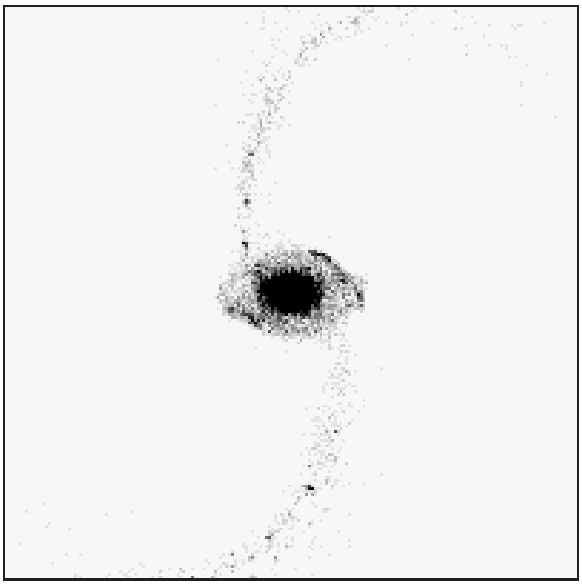

Figure A.1 The Formation of Tidal Tails

The series of two articles examines a total of six cases in which the distance of closest approach and the ratio of the masses of the two galaxies were varied. In all six cases, bridges and tails formed as the test particles were pulled away from the elliptical galaxy by the passing point mass and eventually passed to the far side of the point mass, creating a tail. Tashpulatov found that the test particles travelled along three types of

trajectories. Some of particles travelled around the point mass once and returned to the elliptical galaxy. Others became satellites of the passing galaxy. In all but the closest approaches, Tashpulatov found a third type of path, that a few of the test particles would orbit the passing galaxy a few times and then leave the system forever - "escapers."

Tashpulatov concluded that gravity alone could cause the formation of bridges and tails. At the time, the conventional wisdom was that forces in addition to gravity were necessary for narrow bridges and tails to form between galaxies. He also speculated that during an encounter of two real, three-dimensional galaxies (as opposed to a galaxy and a point mass), a symmetric pair of tails would form behind each galaxy. An examination of Figure A.1 which is a snapshot from the current series of simulations reveals that Tashpulatov's speculation is correct.

Later studies relaxed Tashpulatov's oversimplified assumptions (Toomre and Toomre 1972) and concluded that his understanding of the galactic tails was misguided. These later studies found that the tails were formed through a tidal effect on the far-side of the perturb galaxy, not unlike how the moon induces tides both on the side of the Earth facing the it and the side facing away from it. Regardless, his conclusion that gravity alone could produce the strange features of interacting galaxies became a basis for later work in the field including this thesis.

Collisionless Collapse

The merger of two spiral galaxies, at least in the approach of these simulations, may be considered a special type of collisionless collapse, meaning that the particles that comprise the collapsing object do not collide with each other during the collapse. In this case, the aforementioned particles are stars, and when one considers the size of stars compared to the distance between them, one can see that this is a reasonable assumption. The hypothesis that such a merger can result in the formation of a elliptical galaxy is based in part on the theory of violent relaxation, first elucidated by Lynden-Bell (1967). He found that a distribution of stellar orbits could relax to statistical equilibrium if the stars passed through regions in which the gravitational potential was changing violently enough.

In a recent article, Polyachenko augments Lynden-Bell's work, by recalculating the distribution of stars in energy that a collisionless collapse results in. He uses the fact that in a such a collapse most of the stars will initially end up on radial orbits which are unstable to precession and speculates that this instability leads to a universal energy distribution. In his calculations, he assumes that the collapsing object can be divided into a series of spherical shells and that relaxation proceeds from the center outward with each shell starting to relax only after the previous one has completely relaxed, therefore the potential due to stars within the shell, that is currently relaxing, is constant.

The task is divided into three parts. First is the definition from initial

conditions of the energy distribution of particles on radial orbits (zero angular momentum) on the edge of instability. Second is the derivation of the distribution of the stars in bins of energy and angular momentum from the original distribution under the assumption that the orbits become stable by acquiring a small amount of transverse velocity over a period that is long compared to a single radial orbit. The third part of the task is to integrate this distribution over velocity to obtain the density of stars as a function of radius, which can be observed.

Polyachenko derives a distribution of particles as a function of energy that is in good agreement with numerical simulations of similar processes. However, the distribution does not agree with the results derived by Lynden-Bell. Polyachenko speculates that Lynden-Bell's conclusions are more appropriate for an initially chaotic distribution of particles, while Polyachenko assumes that the initial distribution was cold (i.e. all the particles initially had the same energy). Although Polyachenko's conclusions agree with the numerical simulations, it is also an oversimplification, and the true answer probably lies between these two extremes.

Observations

The work of Vorontsov-Vel'yaminov is among the most extensive in the field of galaxy mergers. He has focused on photographing and classifying interacting galaxies. Since we can never expect to simulate merging galaxies to complete accuracy, this effort is extremely important in gaining a complete

understanding of these phenomena. By cataloging a large sample of interacting galaxies, one can hope to construct a movie of a complete galaxy merger from a series of snapshots in the catalog. Unfortunately and not unexpected, this is a difficult task since galaxy interactions are short-lived and therefore rarely observable phenomena.

How Important Are Interactions?

Many researchers, including Vorontsov-Vel'yaminov (1977), have compared the short interval during which the symptoms of galaxy interactions are apparent (about a billion years) with the number of galaxies that are presently observed to be undergoing an interaction, and have concluded that interactions may play a large role in galactic evolution. Vorontsov-Vel'yaminov contends that during interactions under the action of tidal forces galaxies may drastically change their form and size. During the interaction, spiral and straight limbs, bridges and tails can form, and more importantly for the future of the galaxies, gas may be exchanged or lost entirely. Without gas, a new stars cannot form in a galaxy, and on the other hand an infusion of fresh gas can spark a wave of star formation in a galaxy that would have remained dormant otherwise. He points to the galaxies NGC 4038/39 and NGC 3995 which are experiencing a burst of star formation. He argues that this hyperactivity is a direct result of collisions between these galaxies.

Regardless of the violence of the activity induced by galaxy interactions, interactions cannot play an important role in galactic evolution unless they are

abundant. Vorontsov-Vel'yaminov (1977) estimates the frequency of interactions in the following manner. First he estimates that about 14% of observed galaxies are members of interacting pairs and that an interaction will last at least 10^{8} years. Thus, even when one considers that a single galaxy could be involved in more than one interaction over this period, over the age of the universe (10^{10} years), most galaxies should have experienced an interaction of some sort. He concludes, "This is a quantity which one cannot neglect neither in cosmogony nor in cosmology."

Summary

The contributions of Soviet and Russian researchers in the field of galaxy interactions have been quite substantial. For the most part, these contributions have taken a form wholly different from the approach of this thesis. The realities of the Soviet economy and political system in a way forced Soviet scientists to take the path of observations and analytic theory rather than pursue the route of large-scale numerical simulations. This has made the Soviet contributions and those made elsewhere uniquely complementary.

Bibliography

Arp, H., 1966, *Atlas of Peculiar Galaxies* (Pasadena: California Institute of Technology)

Lynden-Bell, D. 1967, *M.N.R.A.S.*, **136**, 101.

Polyachenko, V.L. 1991, *Pis'ma v Astronomicheskij Zhurnal*, **17**, 691-701.

Tashpulatov, N. 1969, *Astronomicheskij Zhurnal*, **46**, 1236-1246.

Tashpulatov, N. 1970, *Astronomicheskij Zhurnal*, **46**, 277-291.

Toomre, A., and Toomre, J. 1972, *Ap. J.*, **178**, 623.

Vorontsov-Vel'yaminov, B.A. 1959, *Atlas and Catalog of Interacting Galaxies* (Moscow: Sternberg State Astronomical Institute)

Vorontzov-Vel'yaminov, B.A. 1975, *Astrofisika*, **11**, 353-354.

Vorontzov-Vel'yaminov, B.A. 1976, *Pis'ma v Astronomicheskij Zhurnal*, **2**, 515-519.

Vorontzov-Vel'yaminov, B.A. 1977, *Pis'ma v Astronomicheskij Zhurnal*, **3**, 251-253.